EFFECT OF DIVALENT IONS ON THE STRUCTURE OF LAYER BY LAYER ASSEMBLIES

A Dissertation

by

DARIYA KONSTANTINOVNA REID

Submitted to the Office of Graduate and Professional Studies of
Texas A&M University
in partial fulfillment of the requirements for the degree of

DOCTOR OF PHILOSOPHY

Chair of Committee,	Jodie L. Lutkenhaus
Committee Members,	Mustafa Akbulut
	Sam Mannan
	Hung-Jue Sue
Head of Department,	Nazmul Karim

May 2016

Major Subject: Chemical Engineering

ABSTRACT

The effects of ion concentration and type on the structural and fundamental property changes in poly(diallyldimethylammonium chloride) (PDAC) / poly(styrene sulfonate) (PSS) layer-by-layer (LbL) assemblies are investigated. These properties are monitored using quartz crystal microbalance with dissipation (QCM-D) and modulated differential scanning calorimetry (MDSC). PDAC-terminated multilayers reveal concentration dependent thickness changes upon exchange of contact solutions between NaCl and divalent cation salts ($CaCl_2$ and $MgCl_2$). At low concentrations, thickness changes increase with decreasing concentration, while at high ionic strength the opposite trend is observed. Alternatively, the LbL film exhibits similar behavior but no concentration dependence, when in the presence of divalent anion salt (Na_2SO_4). The observed expansion of the films when exposed to divalent ion salts is analyzed in terms of the hydration efficiency of the ions and osmotic pressure. Mechanical properties of the film mirror the structural changes with the film becoming more rigid and bearing a higher shear modulus when in the presence of NaCl. These changes are attributed to the plasticizing effect of water molecules. Thermal changes in hydrated PDAC/PSS assemblies are also monitored with respect to the type of ions present in the hydrating solution and the ionic strength of the solution. Unlike structural behavior, the thermal transition (T_{tr}) observed in hydrated films shifts to higher temperatures with increasing concentration of Na_2SO_4. However, when hydrated with $CaCl_2$ or $MgCl_2$ solutions the

T_{tr} remains constant within standard deviation. The effect of chaotropic/kosmotropic character of the ions is considered when drawing conclusions regarding the T_{tr} behavior.

ACKNOWLEDGEMENTS

I would like to thank my advisor, Dr. Jodie Lutkenhaus, for the support and patience she has shown in teaching me and guiding my research work. I wish to thank Dr. Mustafa Akbulut, Dr. Sam Mannan and Dr. Hung-Jue Sue for serving on my committee and for the provided direction in completing my project.

I would also like to thank my lab mates, past and present, and my friends here at Texas A&M University for their support. I extend my deepest gratitude to my family for their unwavering confidence in my ability to succeed and their encouragement during the toughest and most stressful moments.

This work was supported in part by National Science Foundation CAREER (DMR) Award No 1049706 and NSF Grant No 1312676.

NOMENCLATURE

a	Free water molecules associated with the multivalent cations
A^-	Monovalent anions
A^{n-}	Multivalent anion
AFM	Atomic force microscopy
b	Free water molecules associated with the monovalent anions
C	Sensitivity constant
c, d, g and h	Waters associated with ions forming extrinsic compensation
C^+	Monovalent cations
C_l	Speed of light
C^{n+}	Multivalent cation
C_p	Heat capacity
DMA	Dynamic mechanical analysis
DSC	Differential scanning calorimetry
dT/ dt	Applied heating rate
e	Free water molecules associated with the multivalent anions
$E_{dissipated}$	Reduction in energy during a single oscillation cycle
E_{stored}	Overall energy of the oscillator
f	Free water molecules associated with the monovalent cations
f_F	Fundamental resonance frequency
FTIR	Fourier transform infrared spectroscopy

f(T,t)	Nonreversing heat flow
G’	Shear modulus
G”	Shear loss modulus
IL	Ionic liquid
k	Bond strength between the two atoms
LbL	Layer-by-layer
MDSC	Modulated differential scanning calorimetry
m_1 and m_2	Atomic mass
n	Overtone number
PAA	Poly(acrylic acid)
PAH	Poly(allylamine hydrochloride)
PDAC	Poly(diallyldimethylammonium chloride)
PEI	Polyethylenimine
PEM	Polyelectrolyte multilayers
PEO	Poly(ethylene oxide)
PMAA	Poly(methacrylic acid)
PMETAC	Poly[2-(methacryloyloxy)ethyltrimethylammonium chloride]
Pol^+	Polycation
Pol^-	Polyanion
PSPMA	Poly(3-sulfopropyl methacrylate potassium)
PSS	Poly(styrene sulfonate)
P4VP	Poly(4-vinyl pyridine)

QCM	Quartz crystal microbalance
QCM-D	Quartz crystal microbalance with dissipation
T_{tr}	Thermal transition
x	Water molecules hydrating the intrinsically compensated sites
y	Free water molecules
α' and α"	Frequency dependent modulus parameters
δ	Penetration depth
η_l	Solution viscosity
η	Viscosity
ρ_l	Solution density

TABLE OF CONTENTS

Page

LIST OF FIGURES

Page

LIST OF TABLES

Page

1. INTRODUCTION AND LITERATURE REVIEW

1.1: Layer-by-Layer Assembly Technique

Layer-by-layer (LbL) assemblies are prepared through sequential adsorption of oppositely charged species onto a substrate.[1] The widespread interest in this technique and the growing number of applications has made it the subject of multiple review articles.[2-5] Since its introduction over 20 years ago, the technique has been applied to a variety of substrates and components.[6] Common materials used in the preparation of LbL films are strong and weak polyelectrolytes, due to their diversity and commercial availability. Figure 1 shows multiple sample preparation methods used in LbL assembly including dipping and spraying.

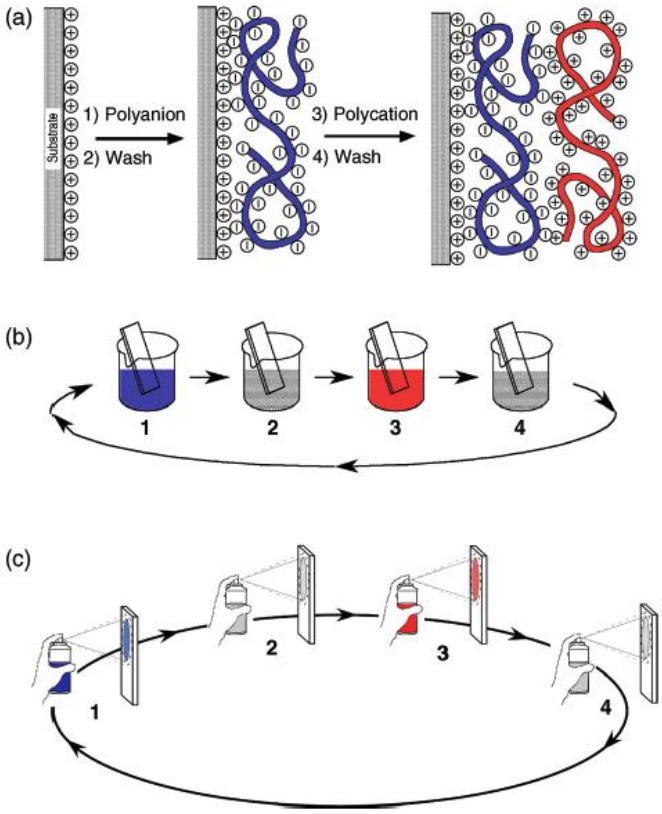

Figure 1. Schematic representation of layer-by-layer assembly using various experimental techniques. From Decher, G., Layer-by-Layer Assembly (Putting Molecules to Work), in Multilayer Thin Films. Copyright © 2012 by Wiley-VCH Verlag GmbH & Co. KGaA. Reprinted by permission of John Wiley & Sons, Inc.

The LbL technique has been broadly used in gas separation applications,[7-8] optical devices,[9] sensors[10-11] and drug delivery.[12-14] A recent review by Richardson *et al.* highlights the versatility the technique possesses and its ability to accommodate each of these applications.[15] Figure 2a shows a wide range of substrates, deposited materials and processing techniques for which LbL assembly is compatible. Figure 2a also illustrates that the substrates and the materials used for the preparation of LbL films can be uniquely selected for an application.[15] A substrate can be either flexible (fabric) or rigid

(silicon wafers) while the materials range from biological molecules to inorganic nanoparticles. Depending on the particular parameters chosen in any of the categories shown in Figure 2 the resultant LbL structure can be applied in areas such as batteries, water purification or tissue engineering.[15]

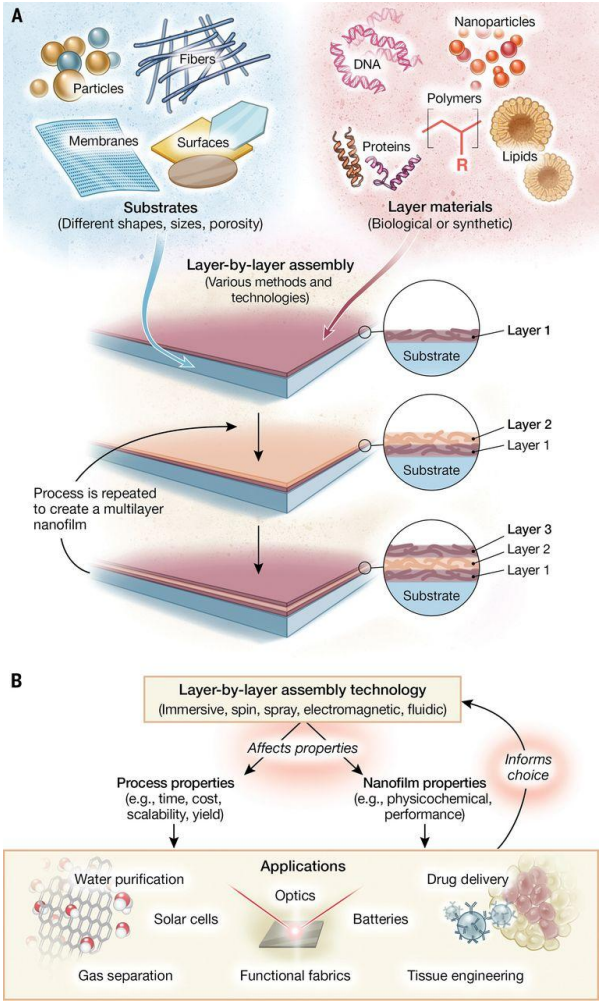

Figure 2. (a) Schematic illustration of the wide variety of variables involved in preparation of LbL assemblies and (b) the resultant technologies that utilize the prepared films. From Richardson, J. J.; Björnmalm, M.; Caruso, F. *Science* 2015, *348*. Reprinted with permission from AAAS.

Hollow capsules prepared using the LbL technique have been of great interest in the field of drug delivery.[16] Successful encapsulation of dextran in hollow poly(allylamine hydrochloride) (PAH) / poly(styrene sulfonate) (PSS) nanocapsules was demonstrated by Sukhorukov *et al*.[17] At low pH values (pH 3) dextran was able to permeate through the LbL film into the hollow interior and the capsule was designated as "open". At high pH values (pH 10) the LbL walls were more compact and did not allow for the passage of dextran, thus the capsule was identified as "closed".[17] In a separate study by Georgieva *et al*. the infiltration of human serum albumin into PSS/PAH capsules was controlled using the ionic strength of the external solution.[18] An interest in antistatic fabric has led researchers to coat cloth with poly(diallyldimethylammonium chloride) (PDAC) and multiwalled carbon nanotubes (MWNT) using the LbL approach.[19] Figure 3a shows that the average value of sheet resistance, collected using a four-point probe, of 1.4×10^6 Ω/□ for the machine-coated fabric is significantly lower than the resistance of 10^{11} Ω/□ for the uncoated fabric. The observed increase in conductivity of the fabric indicates the films' potential as an antistatic coating.[19]

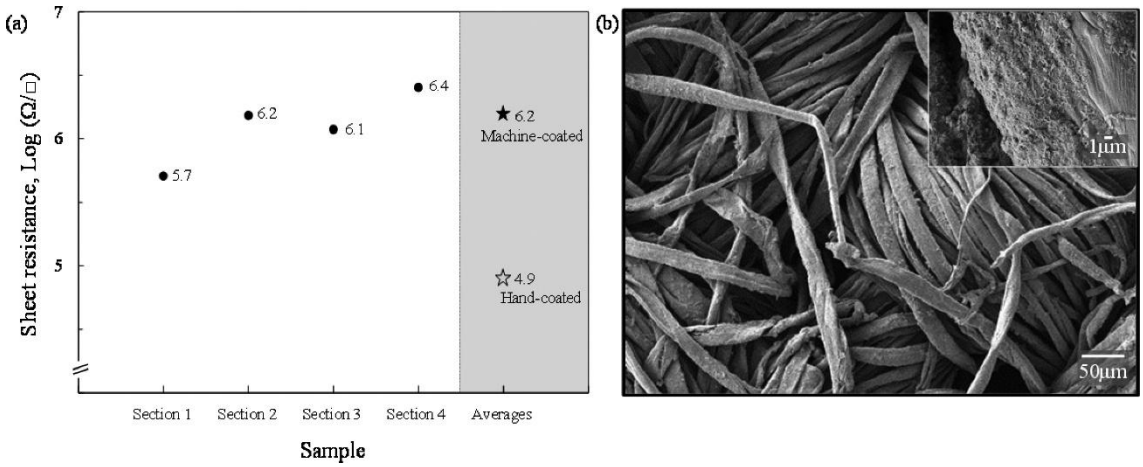

Figure 3. (a) Sheet resistance of a piece of fabric coated with five bilayers of PDAC and MWNT; (b) SEM image of the coated fabric. Reprinted (adapted) with permission from Mateos, A. J.; Cain, A. A.; Grunlan, J. C. *Industrial & Engineering Chemistry Research* 2014, *53*, 6409-6416. Copyright 2014 American Chemical Society.

In order for these types of films to reach their full potential in the presented fields of application a more complete understanding of their structural behavior and mechanical properties under variable conditions is necessary.

While dipping is the most widely used technique, spray-assisted LbL provides the shortest sample preparation time. Several publications focus on determining the differences between the two techniques. Sung *et al.* prepared LbL assemblies composed of poly(ethylene oxide) (PEO) / poly(acrylic acid) (PAA) and PEO / poly(methacrylic acid) (PMAA) using both the dip and the spray method in order to compare the thermal properties of the films.[20] The researchers found that for both systems the spray assembly method resulted in smaller layer pair thickness and larger glass transition breadth. The position of the glass transition remained unaffected by the preparation method.[20] However, others have found that the structure of the LbL films is affected by the

preparation method. An LbL film can have a structure that is interdigitated, which is often the case for films prepared using the dipping method.[15] In such films each additional layer that is deposited onto a substrate penetrates some distance into bulk of the film.[1] Figure 4 is an illustration of a typical LbL film prepared by dipping onto a positively charged substrate. Blue circles represent the polyanion and red circles represent the polycation. Figure 4 also shows that a single layer of a particular charge penetrates as far as half way into the previously deposited layer of the same charge.[1] Recognizing these observations LbL films prepared in this work are considered to be largely homogeneous with some distribution of composition vertically along the film. Laterally the films form a uniform coating and full surface coverage.

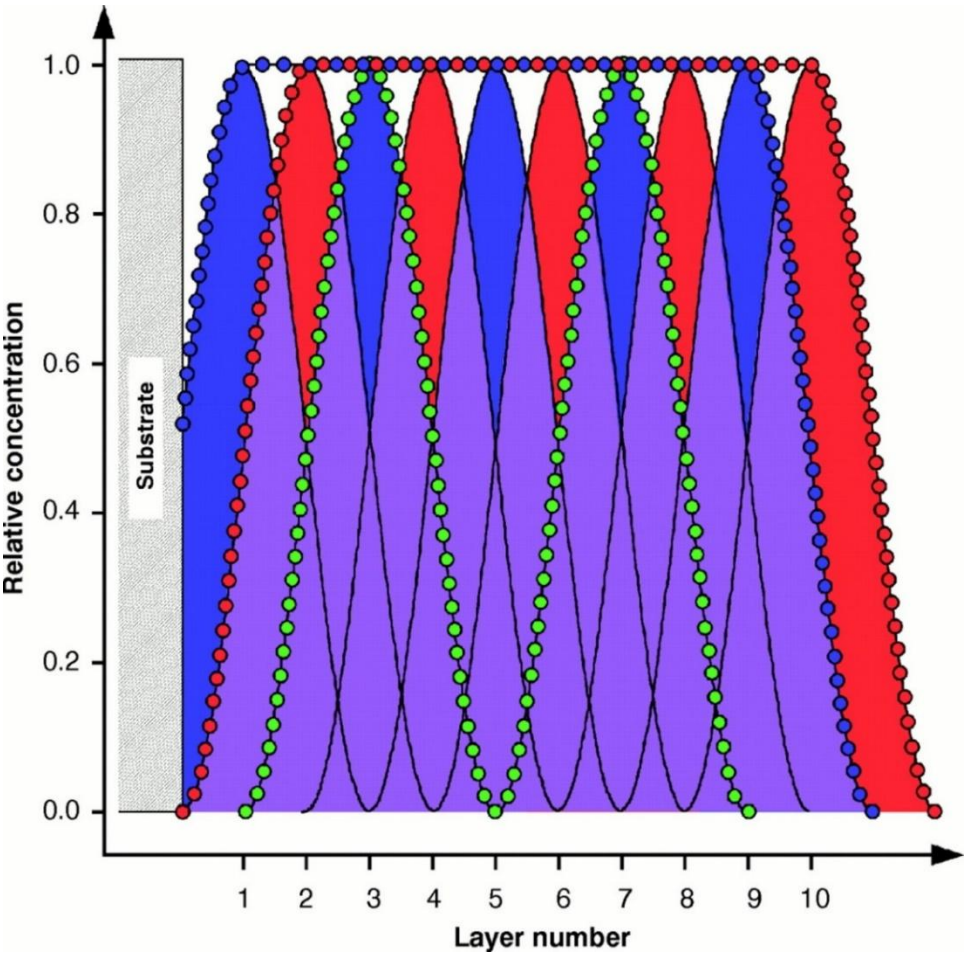

Figure 4. Schematic representation of the distribution of charged layers within an LbL film of ten bilayers. From Decher, G. *Science* 1997, *277*, 1232-1237. Reprinted with permission from AAAS.

Unlike dip-assisted LbL assembly, spin-assisted LbL assembly produces films that bear distinct layers and a stratified structure which in turn affects other physical properties of the film. Seo *et al*. demonstrated that multilayer films prepared using hydrophobically modified PEO (HM-PEO) and PAA bore strikingly different surface properties when prepared using the dip-assisted and the spin-assisted method.[21] The researchers found the spin-assisted method produced much smoother films. The roughness of a fifty bilayer

film is reported as less than one nm compared to an average roughness of 4000 nm for a dip-assisted film.[21] Figure 5 illustrates the stark differences in the transparency of free-standing films deposited by dip-assisted and the spin-assisted assembly. The opacity of the dip-assisted film is related to the surface roughness while the transparency of the spin-assisted film is attributed to the stratified nature of the film.[21]

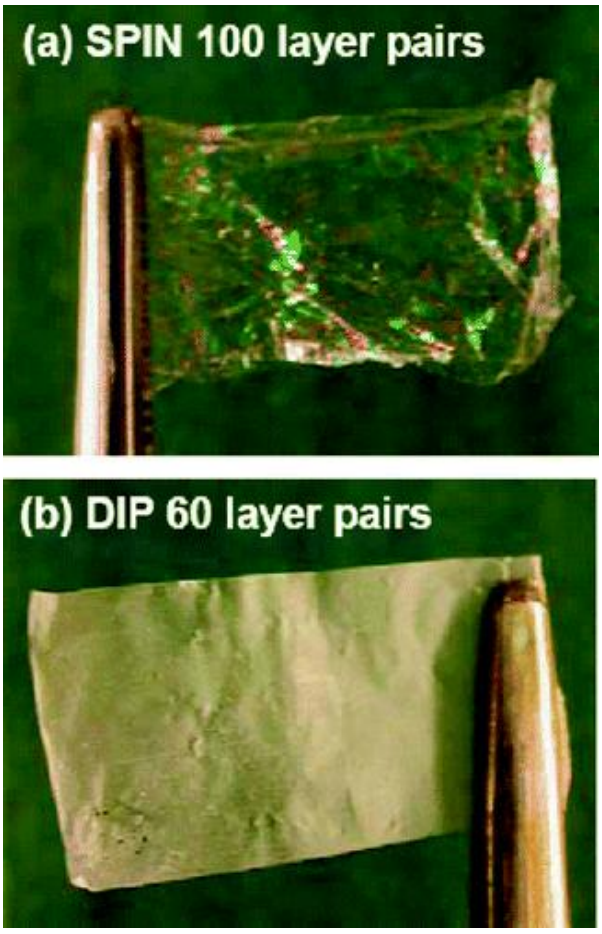

Figure 5. (a) Photos taken of a one hundred bilayer free-standing HM-PEO/PAA film prepared using spin assembly and (b) a sixty bilayer HM-PEO/PAA film prepared using dipping. Reprinted (adapted) with permission from Seo, J.; Lutkenhaus, J. L.; Kim, J.; Hammond, P. T.; Char, K. *Langmuir* 2008, *24*, 7995-8000. Copyright 2008 American Chemical Society.

A number of other controlling factors affect the structure of an LbL film as well as its properties. These tuning parameters include pH,[22-23] temperature,[24-26] solvent type,[27-28] ionic strength[29-30] and counter ion type.[27, 31-34] Dubas *et al.* studied the effect of ion type, among other parameters, on the thickness of PSS/PDAC LbL assemblies. The researchers studied both a collection of anions (Na^+ as the cation) and a collection of cations (Cl^- as the anion). The overall conclusion of the work was that the use of ions with lower hydration number led to thicker films.[27] Additional studies performed using quartz crystal microbalance with dissipation (QCM-D) on the same system concluded that PDAC/PSS film growth proceeded nonlinearly when using Br^-, ClO_3^-, and Cl^- due to the effect of the anion on chain interpenetration within the film. [31] The relative screening efficiency of each individual ion affects the swelling of the PDAC layer which allows the PSS chains to penetrate into the film more easily. Figure 6 shows that films built up using F^-, CH_3COO^-, $H_2PO_4^-$, and SO_4^- as the counterion resulted in linear growth due to changes in polyelectrolyte conformation.[31] Linear growth arose from the screening effect of the counterions on the conformation of the terminal layer of PDAC.[31]

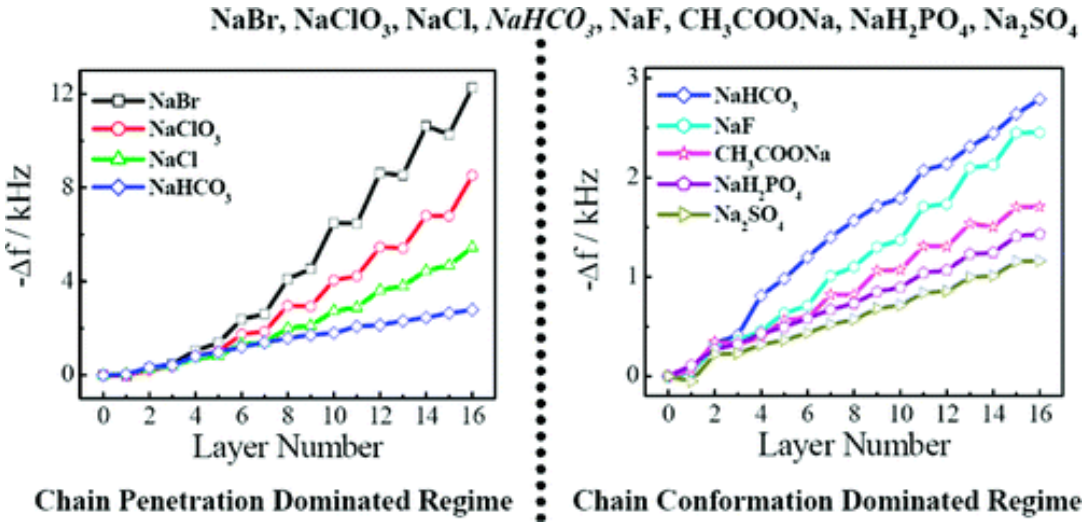

Figure 6. Changes in frequency collected using QCM-D as a function of layer number showing the effect of counterion selection on the growth of PDAC/PSS multilayers. Reprinted (adapted) with permission from Liu, G.; Hou, Y.; Xiao, X.; Zhang, G. *The Journal of Physical Chemistry B* 2010, *114*, 9987-9993. Copyright 2010 American Chemical Society.

Shiratori *et al.* prepared PAA/PAH multilayer films ranging in bilayer thickness from < 10 Å to > 120 Å.[22] The data set was collected for two conditions: 1) pH of PAH solution was kept constant while the pH of the PAA solution was adjusted between 2.5 and 9 and 2) pH of PAA solution was kept constant while the pH of the PAH solution was adjusted over the same range.[22] Figure 7 is a summary of the bilayer thickness over the full collection of pH conditions. From the graph it is apparent that the lowest film thickness resulted when the pH of the PAA solution was high and the pH of the PAH solution was low.[22] Ultra-low thicknesses are obtained when the surface charge of a deposited layer is reversed by the pH of the solution that is adsorbing as the next layer. Higher thicknesses

are attributed to the more compact conformation of the polyelectrolyte chains as they deposit onto the surface.[22]

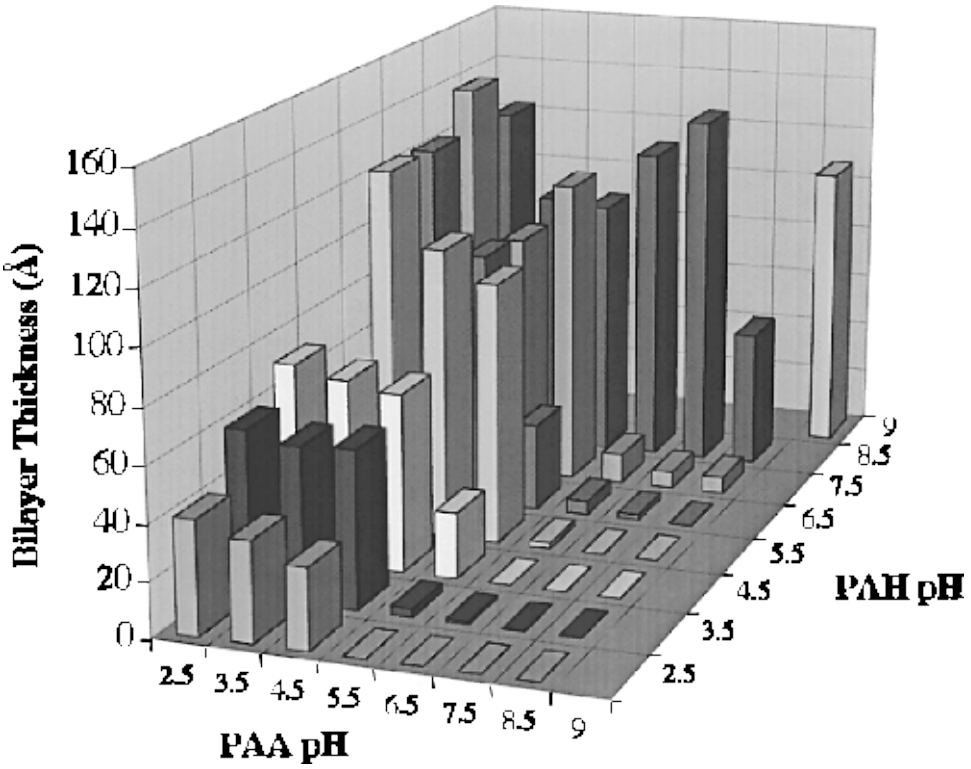

Figure 7. Effect of solution pH on the growth of PAA/PAH multilayers. Reprinted (adapted) with permission from Shiratori, S. S.; Rubner, M. F. *Macromolecules* 2000, *33*, 4213-4219. Copyright 2000 American Chemical Society.

1.2: Physical Properties of Layer-by-Layer Assemblies

1.2.1: Structural Changes

In recent years significant advances have been made in understanding the swelling of LbL multilayers under a range of conditions.[35-46] Ionic strength was shown to have a significant impact on the structure of LbL assemblies in a number of studies.[39-40] Figure 8 shows hollow microcapsules prepared from nine layers of PSS/PDAC and terminated with PDAC that were observed to fluctuate in diameter with changing ionic strength. As prepared capsules had a diameter of ≈ 4.5 μm. Confocal images in Figure 8a display an increase in capsule diameter when placed in 1 – 10 mM salt solutions.[39] However, in a higher ionic strength environment (30 mM and 100 mM) the capsule diameter decreased. At low ionic strengths and minimal charge screening the electrostatic forces cause capsule expansion.[39] While the observed contraction stems from the hydrophobic nature of the polyelectrolytes and the drive to minimize the interactions between the polyelectrolyte chains and the solvent. The diameter also marginally increased as the temperature was ramped from 40 to 60 ^{o}C due to a reduction in surface tension.[39]

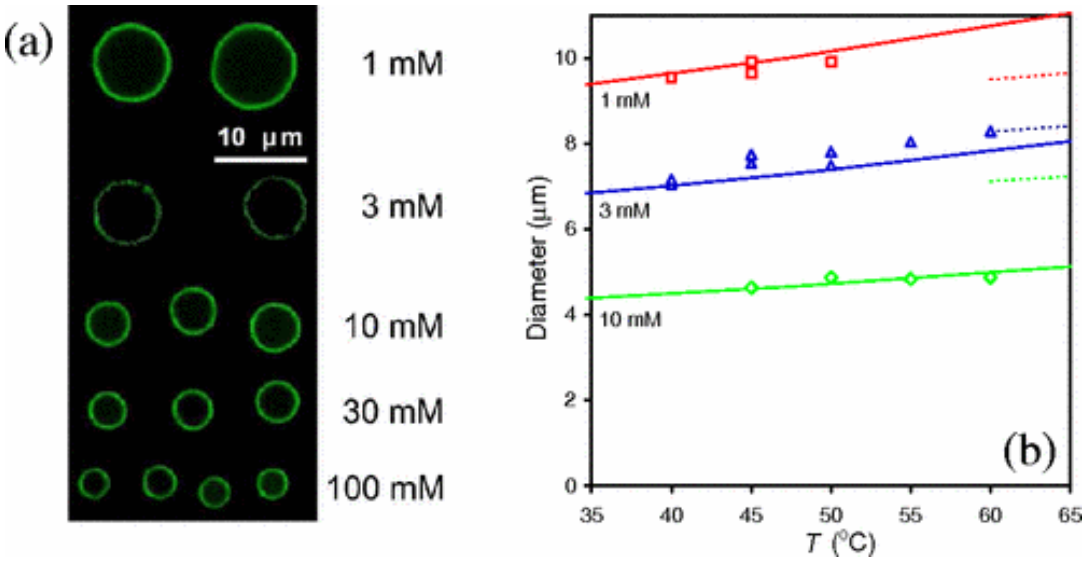

Figure 8. (a) Confocal images of the changing diameter of PSS/PDAC hollow microcapsules taken in solutions of varying ionic strength. (b) Capsule diameter as a function of temperature. Reprinted figure with permission from Köhler, K.; Biesheuvel, P. M.; Weinkamer, R.; Möhwald, H.; Sukhorukov, G. B. *Physical Review Letters* 2006, *97*, 188301. Copyright 2006 by the American Physical Society.

A reduction in surface roughness of PDAC/PSS LbL films through annealing in salt solutions was demonstrated by Dubas *et al*.[40] Figure 9 shows atomic force microscopy (AFM) images of the surface of a ten bilayer PDAC/PSS multilayer film before and after annealing in 1 M NaCl solution for four hours. From AFM analysis it was concluded that the roughness decreased from about 15 nm to less than 5 nm after annealing in 1 M NaCl for up to 400 min. [40] The study also revealed two-stage swelling phenomena for PDAC/PSS multilayers. At low ionic strength the films contracted with increasing salt concentration due to an external osmotic pressure effect. As the salt concentration was further increased the film began to swell due to water and ion uptake.[40]

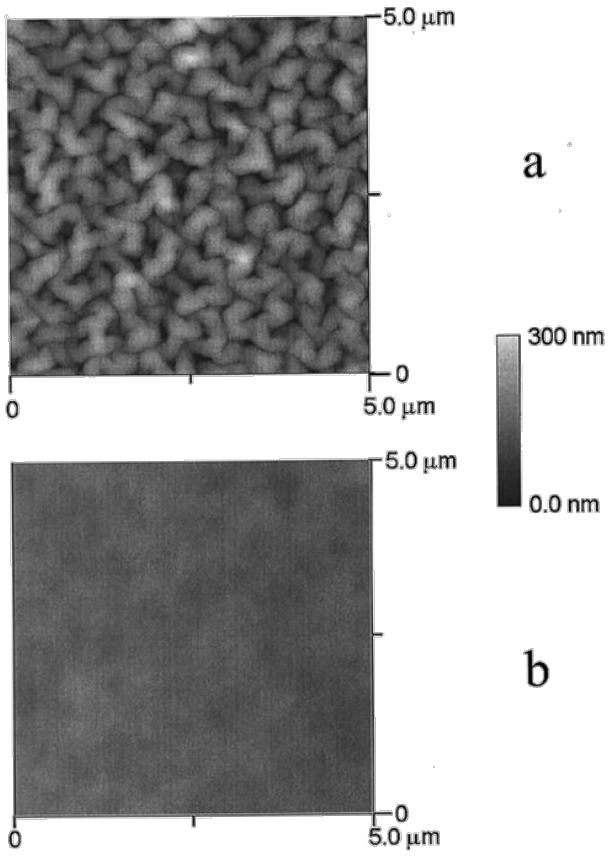

Figure 9. Reduction in surface roughness observed by AFM of a PDAC/PSS LbL film. Reprinted (adapted) with permission from Dubas, S. T.; Schlenoff, J. B. *Langmuir* 2001, *17*, 7725-7727. Copyright 2001 American Chemical Society.

The terminating layer has also been shown to influence the post-assembly behavior of LbL films.[38, 41] Top layer-dependent structural collapse of PDAC/PSS films prepared from 0.5 M NaCl was shown using QCM-D. PDAC-terminated LbL assemblies showed a significant reduction in thickness when placed in aqueous NaCl solutions of increasing ionic strength. The films expelled 50% of the water when placed in contact with 1 M NaCl solution. While, PSS-terminated assemblies showed no ionic strength dependence.[38]

Changes in structure of the LbL multilayers have also been observed in relation to the nature of the counterions used during film assembly. Salomaki *et al.* observed that the thickness of films formed from NaF solutions did not show significant change upon exposure to solutions of increasing ionic strength and changing anion.[47] However, films prepared using NaBr showed an increase in thickness upon ion exchange and changing ionic strength.[47] The Hoffmeister series was initially used to rank ions based on their effectiveness in precipitating proteins. This series has also been used to rank the interactions of ions with water.[48] Figure 10 illustrates that the amount of mass change observed in films prepared using NaBr followed the Hoffmeister series with F^- displaying the largest increase and NO_3^- the smallest. [47] Hydration entropy was used as a measure of binding affinity of the anion to PDAC. The fluorine ion has the lowest binding affinity of the measured anions and exposure of the film to NaF causes the greatest uptake of water molecules. Quartz crystal resonator (QCR) was used as the analytical tool.[47]

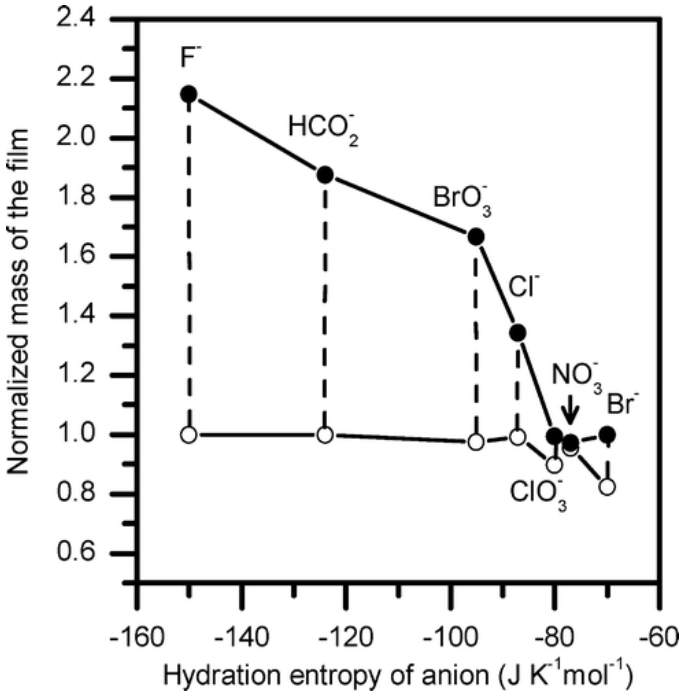

Figure 10. Normalized mass collected using QCR, of a PDAC/PSS LbL film prepared from NaF (open circles) and NaBr (filled circles) after exposure to solutions of various anions as a function of the hydration entropy of the anion. Reprinted (adapted) with permission from Salomäki, M.; Kankare, J. *Macromolecules* 2008, *41*, 4423-4428. Copyright 2008 American Chemical Society.

Dodoo *et al.* observed swelling of dry PDAC/PSS LbL assemblies upon exposure to pure water after assembly from NaF, NaCl and NaBr at different concentrations.[49] The thickness and the amount of incorporated water was larger in films prepared from solutions of higher ionic strength or containing counterions of larger diameter.[49] These results show that the structure of LbL assemblies is highly influenced by the ionic strength and the type of ions that are present in solution during the film build-up process and in contact with the film post-assembly.

1.2.2: Mechanical Properties

The structural response of LbL assemblies to changes in the physical environment is often accompanied by changes in the mechanical properties. Two of the most common parameters reported in literature for polyelectrolyte multilayer systems are the Young's modulus and the shear modulus. Both are mechanical properties of elastic materials and are measured as stress over strain. However, for Young's modulus the stress is tensile and for shear modulus shear stress is applied.

Young's modulus is often measured using AFM for LbL systems. Heuvingh *et al*. prepared PSS/PAH hollow capsules which were then immersed in solutions of varying ionic strength and salt type.[50] Changes in the dimensions and shape of the capsules as well as their mechanical properties were monitored with respect to the chosen parameters. Comparing among the different salt types, SO_4^{2-} had the smallest effect on capsule diameter and NO_3^- had the strongest.[50] Regardless of the salt type as the ionic strength of the solutions increased the diameter of the capsules decreased. Figure 11 shows a corresponding reduction in the Young's modulus with increasing ionic strength.[50] The initial elastic response is constant with a sudden drop between 2.7 M and 3 M NaCl. The authors attribute the softening of the capsules to improved chain rearrangement.[50]

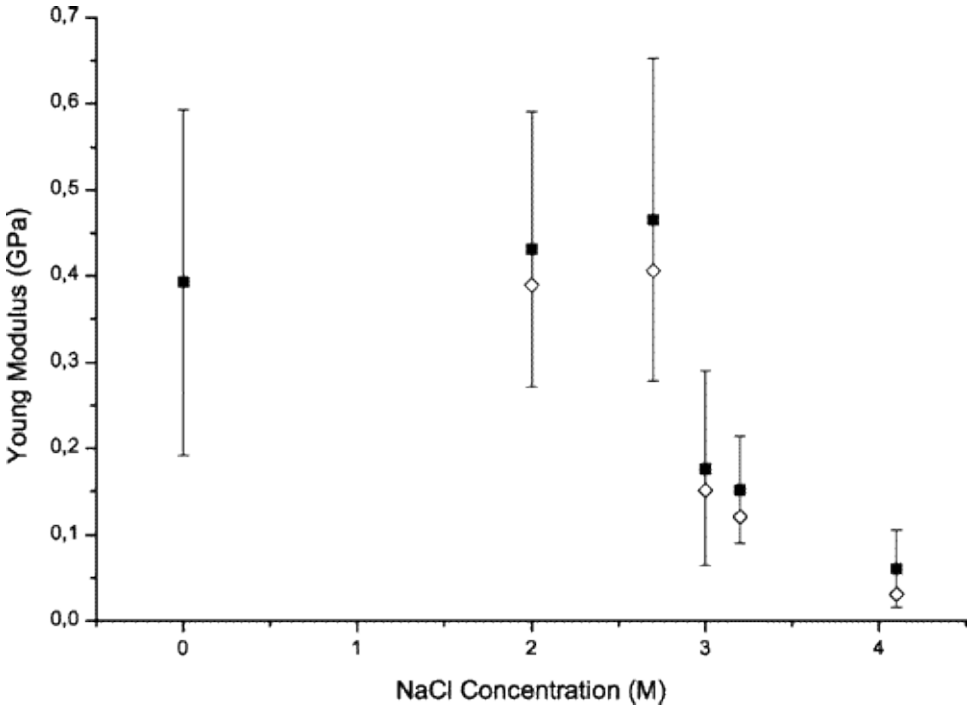

Figure 11. Young's modulus obtained by AFM of PSS/PAH capsules as a function of ionic strength. Reprinted (adapted) with permission from Heuvingh, J.; Zappa, M.; Fery, A. *Langmuir* 2005, *21*, 3165-3171. Copyright 2005 American Chemical Society.

In a separate study Mueller *et al*. examined the effect of temperature on the stiffness of PDAC/PSS hollow capsules.[51] Using confocal imaging the researchers observed a reduction in the capsule diameter with increasing temperature. Figure 12 shows a sharp drop in the stiffness of the capsules at higher temperatures, indicative of a transition from a glassy to a molten state, followed by a plateau starting at about 45 ^{o}C.[51]

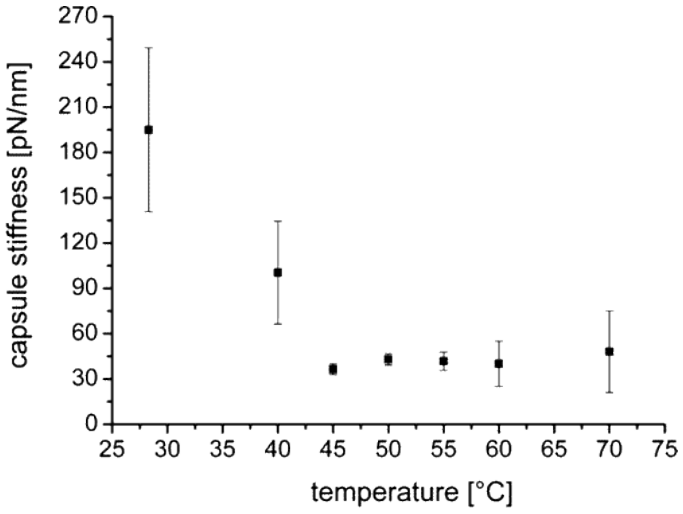

Figure 12. Stiffness of PDAC/PSS capsules as a function of temperature, obtained using AFM. Reprinted (adapted) with permission from Mueller, R.; Köhler, K.; Weinkamer, R.; Sukhorukov, G.; Fery, A. *Macromolecules* 2005, *38*, 9766-9771. Copyright 2005 American Chemical Society.

Dynamic mechanical analysis (DMA) is another convenient tool for measuring mechanical properties. A study performed by the Schlenoff group collected storage and loss modulus measurements of PDAC/PSS LbL films immersed in salt solutions of varying concentrations.[52] As is shown in Figure 13, the storage modulus decreased as the ionic strength of the solution was increased from 0 to 1 M. The general range of elastic modulus was found it to be on the order of 1-25 MPa.[52]

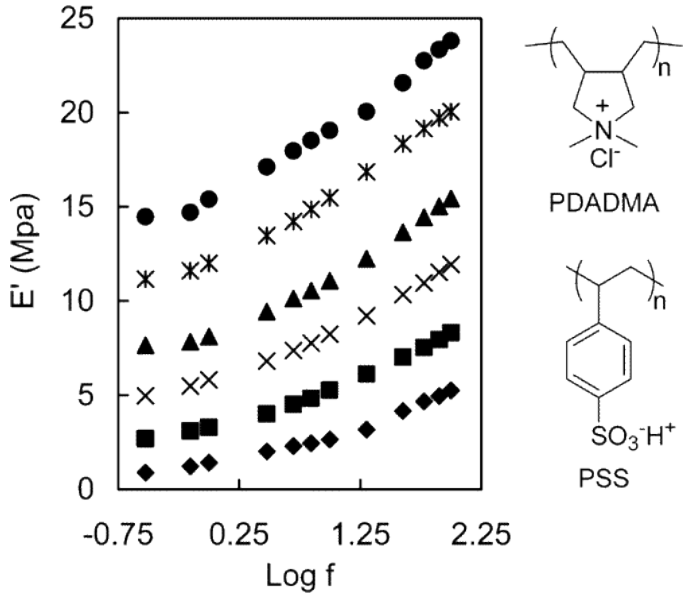

Figure 13. Storage modulus of hydrated PDAC/PSS multilayers as a function of frequency. The symbols from top to bottom represent immersive salt solutions of 0, 0.2, 0.4, 0.6, 0.8 and 1 M concentrations. Reprinted (adapted) with permission from Jaber, J. A.; Schlenoff, J. B. *Chemistry of Materials* 2006, *18*, 5768-5773. Copyright 2006 American Chemical Society.

QCM with impedance detection has been previously used to collect shear modulus measurements of LbL assemblies. Salomäki *et al*. investigated the effect of counterion selection during the film build-up of PDAC/PSS multilayers on the films' elastic response.[53] Under all of the studied conditions the shear modulus of the PDAC/PSS film was on the order of 2 – 100 MPa, similar to the elastic modulus values mentioned previously. Figure 14 shows the reported shear modulus values for a number of PDAC/PSS films prepared using a collection of counterions and how they compare relative to the hydration entropy of the counterions.[53] Hydration entropy is an energy term which relates to the association of water molecules surrounding a particular ion.[54] In this case, hydration entropy is used to arrange the ions according to their influence on

the structure of water molecules within the LbL film. The authors compare the sharp increase in the shear modulus from BrO_3^- to NO_3^- to a glass transition, upon which the material becomes more rigid similar to a glass.[53]

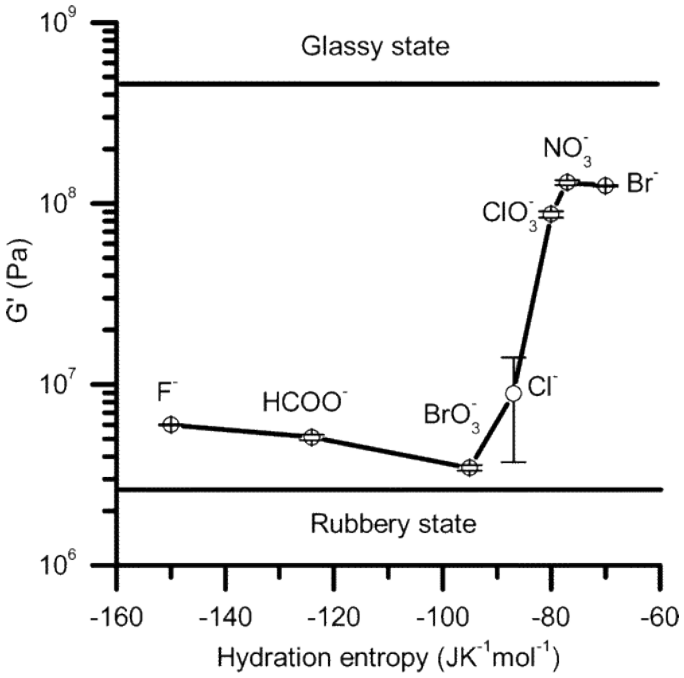

Figure 14. Shear modulus collected using QCM of a PDAC/PSS multilayer film as a function of the hydration entropy of the counterions used during the film build-up. Reprinted (adapted) with permission from Salomäki, M.; Laiho, T.; Kankare, J. *Macromolecules* 2004, *37*, 9585-9590. Copyright 2004 American Chemical Society.

1.3: Thermal Properties

Thermal properties of LbL assemblies have been investigated for a number of systems and a wide range of impactful parameters. Particularly, the film's thermal behavior is affected by changes in hydration state. Vidyasagar *et al*. has previously

demonstrated that free-standing PDAC/PSS multilayers undergo a thermal transition when in the hydrated state which is not observed for dry films, Figure 15.[55] This transition has been observed using both modulated differential scanning calorimetry (MDSC) and QCM-D. Figure 15c also shows that the thermal transition is only evident in films which were prepared in the presence of salt. The ionic strength of the solutions used to prepare the LbL multilayers does not affect the position of the transition.[55]

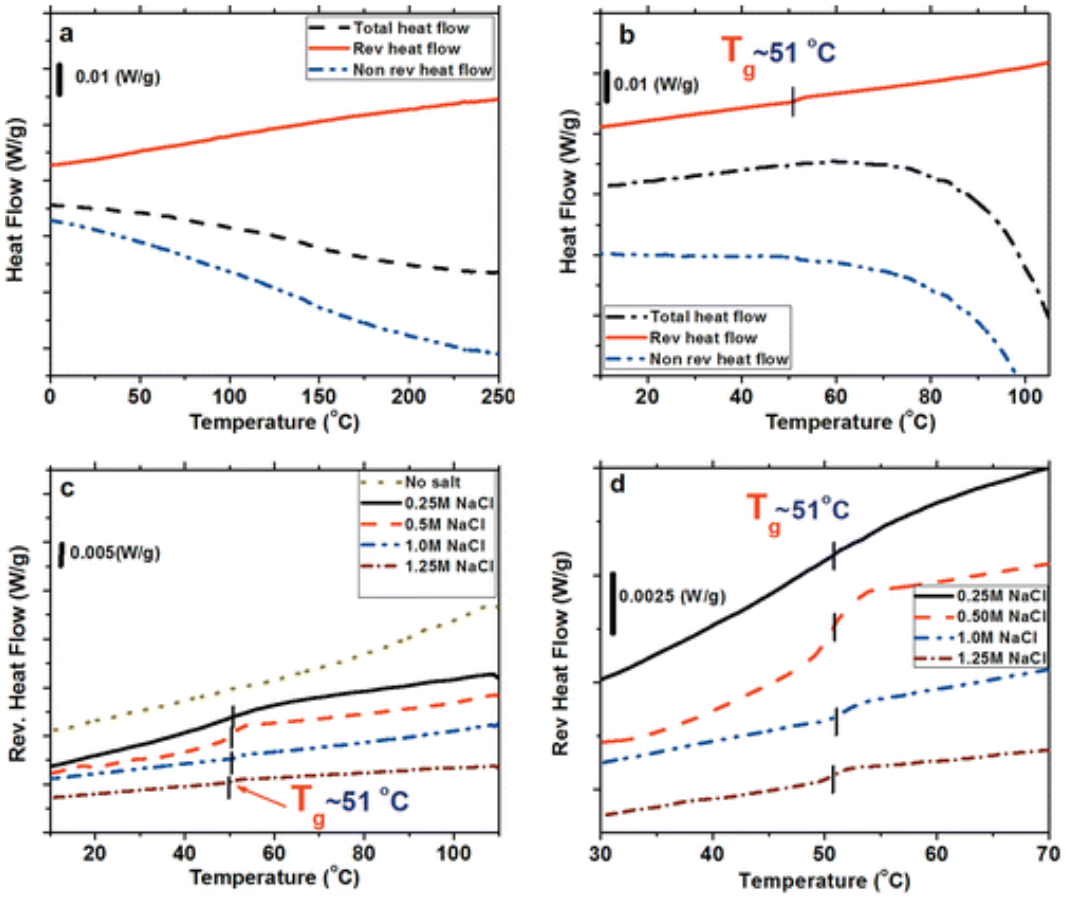

Figure 15. MDSC scans of (a) dry PDAC/PSS LbL films and (b) PDAC/PSS multilayers in the presence of aqueous solutions. Reprinted (adapted) with permission from Vidyasagar, A.; Sung, C.; Gamble, R.; Lutkenhaus, J. L. *ACS Nano* 2012, *6*, 6174-6184. Copyright 2012 American Chemical Society

In addition, recent simulations work from the Sammalkorpi group on PDAC/PSS polyelectrolyte complexes has attributed this transition to the rearrangement of water molecules around the polyanion.[56] Figure 16b shows a reduction in the number of hydrogen bonding interactions between the PSS monomer units and the water molecules. The sharp drop which is observed between 67 and 72 ^{o}C can be matched to the thermal transition observed experimentally in PDAC/PSS assemblies.[56] This glass transition-like behavior comes as result of the breaking of the hydrogen bonding network between the sulfonate groups and the water molecules which results in greater mobility of the PSS chains.[56]

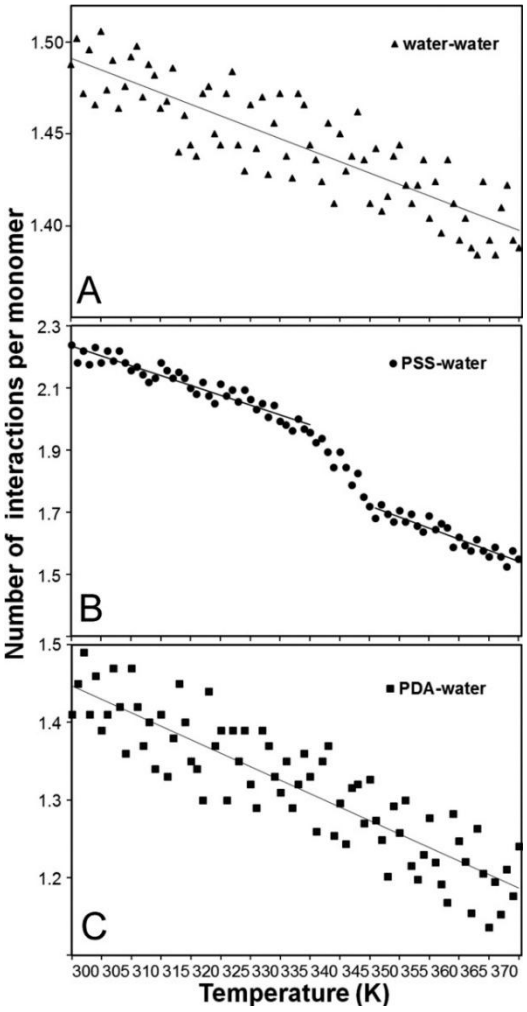

Figure 16. The number of interactions, obtained from molecular dynamics simulations, between (a) water-water, (b) PSS-water and (c) PDAC-water as a function of temperature. Reprinted (adapted) with permission from Yildirim, E.; Zhang, Y.; Lutkenhaus, J. L.; Sammalkorpi, M. *ACS Macro Letters* 2015, *4*, 1017-1021. Copyright 2015 American Chemical Society.

The presence of the transition was further confirmed using electrochemical impedance spectroscopy. Sung *et al.* collected a series of impedance measurements over a temperature range which were converted to charge transfer and film resistances using a modified Randles equivalent circuit. [57] In Figure 17 both resistance values showed a

sharp change in the temperature range which has been previously reported as the thermal transition in the MDSC studies. From the charge transfer resistance data it was evident that the thermal transition decreased with increasing film thickness. The thermal transition was also consistently lower for films prepared using 0.5 M NaCl solutions as compared to 1 M NaCl films.[57]

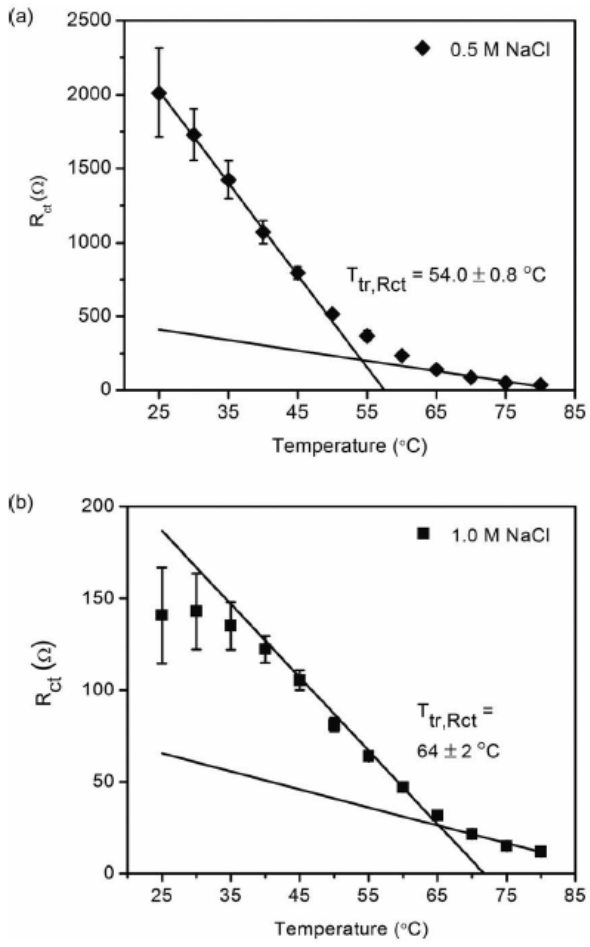

Figure 17. Charge transfer resistance collected using impedance spectroscopy as a function of temperature for PDAC/PSS multilayers prepared using (a) 0.5 M NaCl and (b) 1 M NaCl solutions (b). Reproduced from Ref. 57 with permission from The Royal Society of Chemistry.

The work looking into the thermal transition of PDAC/PSS LbL films was further broadened by looking at the effect of filler materials on the transition. Puhr *et al*. looked at the effect of placing Laponite RD (clay) and Ludox TM-40 (silica) nanoparticles at intermediate positions within the LbL assemblies on the thermal transition of the film using QCM-D.[58] Both the nature of the nanoparticles and their relative location along the structure of the film had a strong effect on the thermal transition. As shown in Figure 18 in the case of the silica nanoparticles the transition only appeared when the particles were placed at the center of the film; in which case, three distinct transitions were evident.[58]

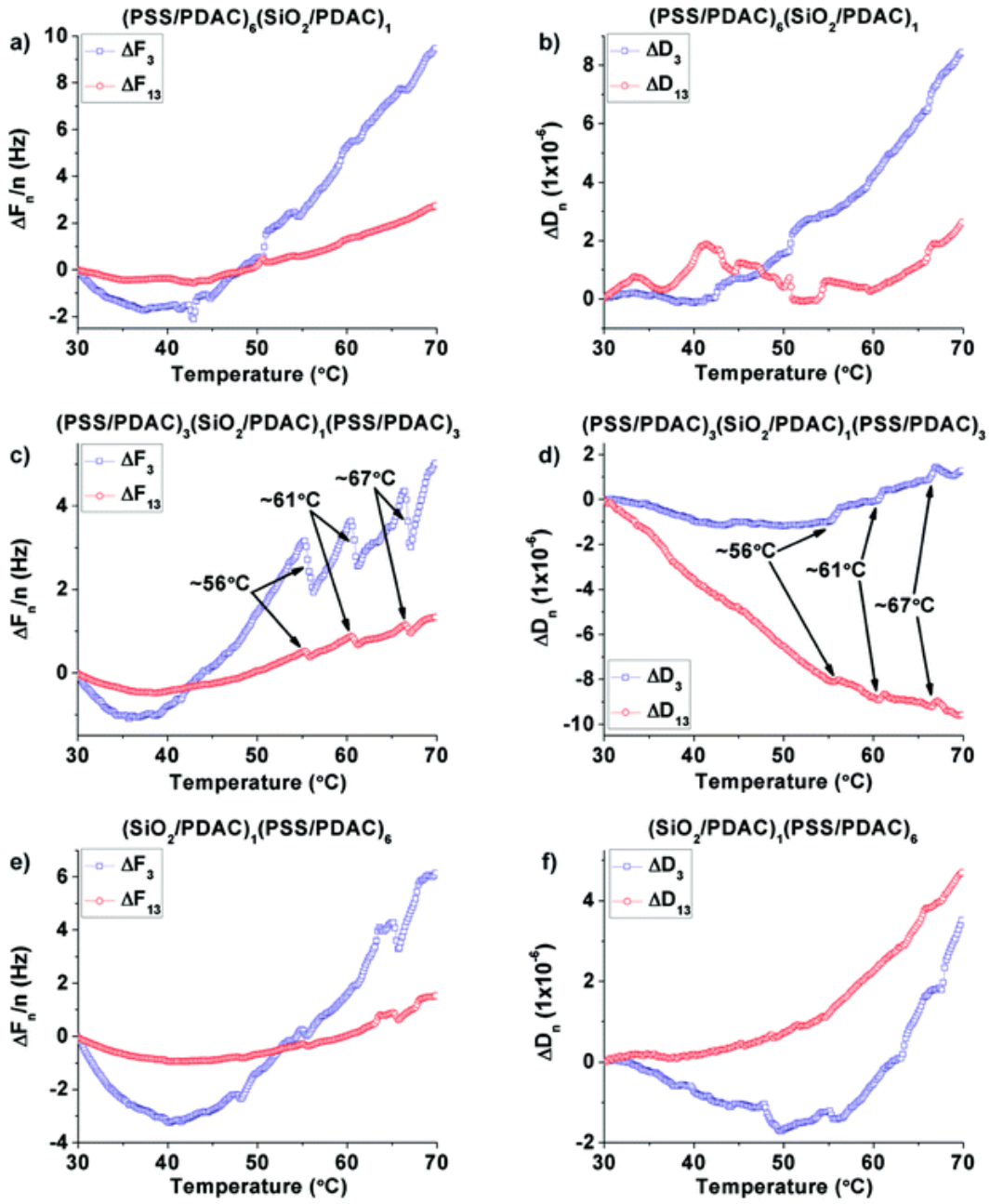

Figure 18. Frequency and dissipation changes observed using QCM-D during the thermal treatment of PDAC/PSS multilayers with SiO_2 particles integrated at different positions within the film structure. Reproduced from Ref. 58 with permission from The Royal Society of Chemistry.

When the film included clay nanoplatelets in the middle or as the terminating layer two distinct transitions were seen; a single transition was recorded when the nanoparticles were located closer to the substrate.[58] In all of the arrangement cases the lower temperature transition was assigned as the "bulk" thermal transition. The higher temperature shifts were associated with the nanoparticles inhibition of polyelectrolyte chain mobility.[58]

1.4: Motivation

The formation of LbL assemblies using model strong polyelectrolytes PDAC and PSS has been well studied for assemblies built-up using NaCl. We are interested in learning how multivalent ions impact the post-assembly structure of LbL multilayers. In addition, when hydrated these films exhibit a thermal transition with features of a glass transition. The question remains as to how multivalent ions affect the nature of the transition.

It is hypothesized that the ion valency would affect the amount of water that penetrates into the film. For example a Ca^{2+} ion is expected to be surrounded by a larger hydration shell as compared to Na^{+}. This may alter the film's structure and properties.

2. QUARTZ CRYSTAL MICROBALANCE WITH DISSIPATION OVERVIEW

2.1: Background

Quartz crystal microbalance, or QCM, is an experimental technique which has been used for over 50 years to monitor changes in mass interacting with a rigid surface.[59] The technique has an incredible accuracy of nanograms and its performance stems from the piezoelectric nature of quartz.[60] The instrument records changes in the frequency of a periodically oscillating quartz crystal as mass deposits onto its surface. Oscillation is achieved by applying an alternating voltage, while the change in frequency is measured in reference to the resonant frequency of the quartz crystal (5 MHz).[60] The recorded changes in frequency can then be converted to thickness or mass measurements using an appropriate model. In 1980 Konash *et al.* expanded the use of QCM by applying it to liquid phase experiments.[61] QCM is now used in a wide variety of applications including protein adsorption, [62] electrochemical applications[63] and thin film preparation.[64] Another major breakthrough occurred with the development of quartz crystal microbalance with dissipation, or QCM-D. In addition to monitoring the changes in frequency QCM-D also records the reduction in the oscillation, or the dissipation, after a voltage has been applied.[60] Dissipation is expressed as:

$$D = \frac{E_{dissipated}}{2\pi E_{stored}}$$

where $E_{dissipated}$ is the reduction in energy during a single oscillation cycle and E_{stored} is the overall energy of the oscillator.[60] This supplementary feature allows for better estimation of thickness for viscoelastic materials as well as determination of additional properties including shear modulus and viscosity. As is shown in Figure 19, change in frequency is coupled to mass or thickness changes. A decrease in frequency is observed as more material is deposited onto the crystal. While the change in dissipation is coupled to viscoelastic properties, an increase in dissipation indicates that the deposited material softens and a decrease in the dissipation is suggestive of a rigid material.

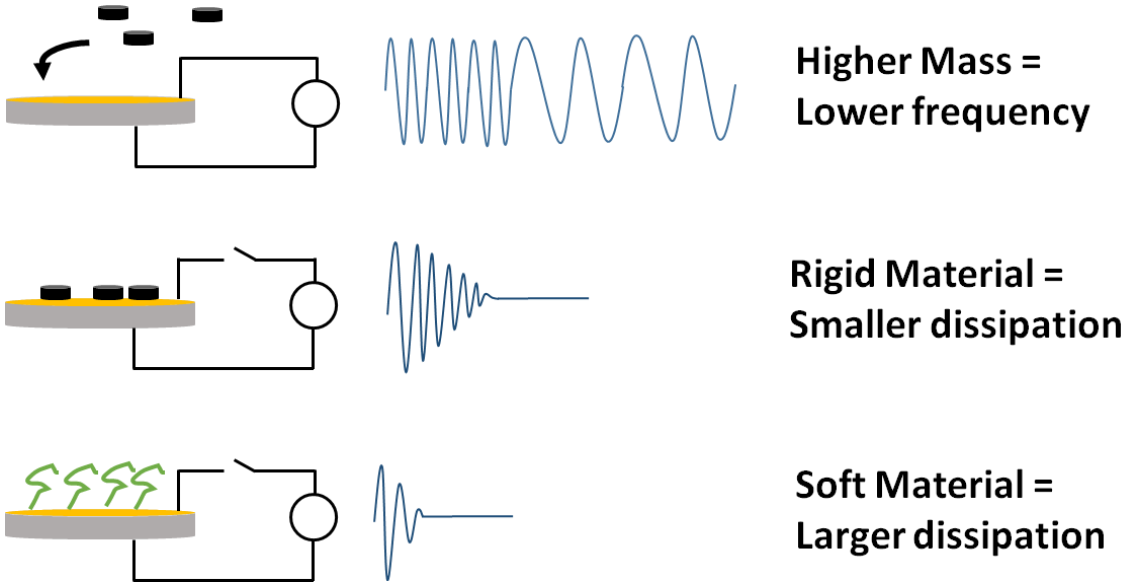

Figure 19. Schematic representation of changes in frequency and dissipation of oscillations upon material deposition. Adapted from Biolin Scientific by Dariya Reid.

2.2: Methodology

In a typical experiment a sample of interest is assembled using a flow through cell. Further details of sample assembly are detailed at the end of this section. QCM-D records the changes in frequency and dissipation as a function of time and overtone number (n = 3, 5, 7, 9, 11 and 13). Each overtone resonates at a different frequency and probes the sample at a different depth. Figure 20 shows schematically the penetration depth observed at different overtones. In pure water penetration depth is estimated to be 250 nm at 5 MHz.[65]

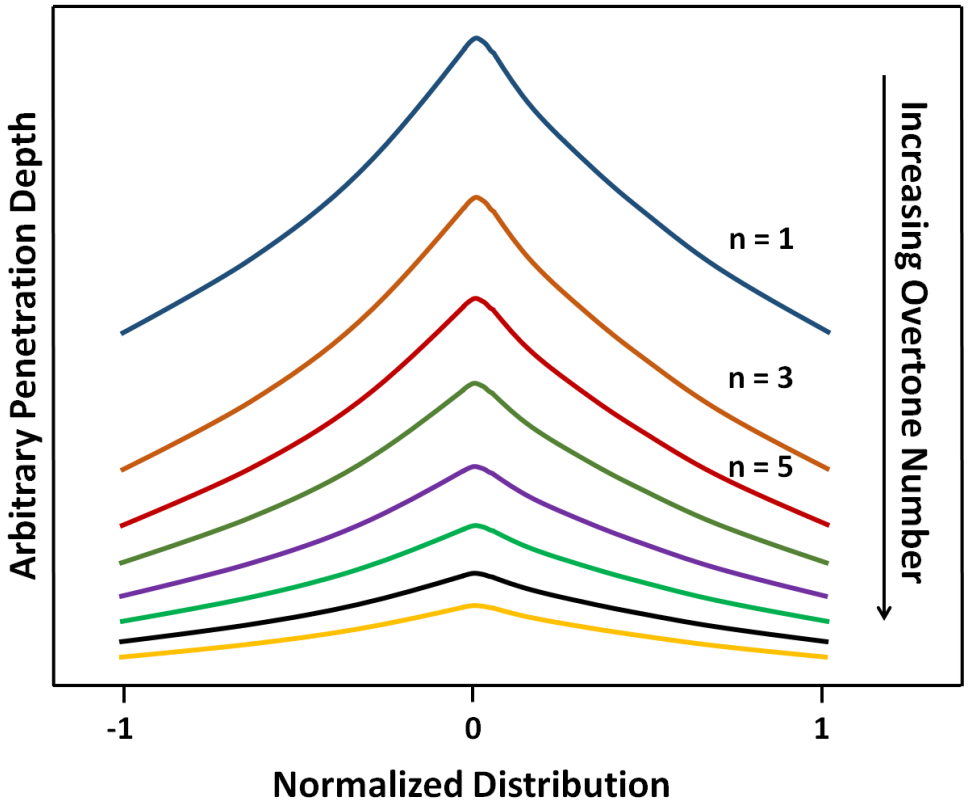

Figure 20. Signal penetration depth for a series of overtones. Adapted from Biolin Scientific by Dariya Reid.

The penetration depth of a solution can be found using the following equation:

$$\delta = \sqrt{\frac{2\eta_1}{2\pi n f_F \rho_1}}$$

where η_l is the solution viscosity, ρ_l is the solution density, f_F is the fundamental resonance frequency and n is the overtone number.[65]

Additionally, the detection sensitivity of the instrument varies with the overtone number as well as with position on the crystal surface. From Figure 21 it is evident that the signal amplitude is optimum for material located at the center of the quartz crystal and is reduced moving out along the radius towards the edges of the crystal. The amplitude range also narrows as the overtone number increases.

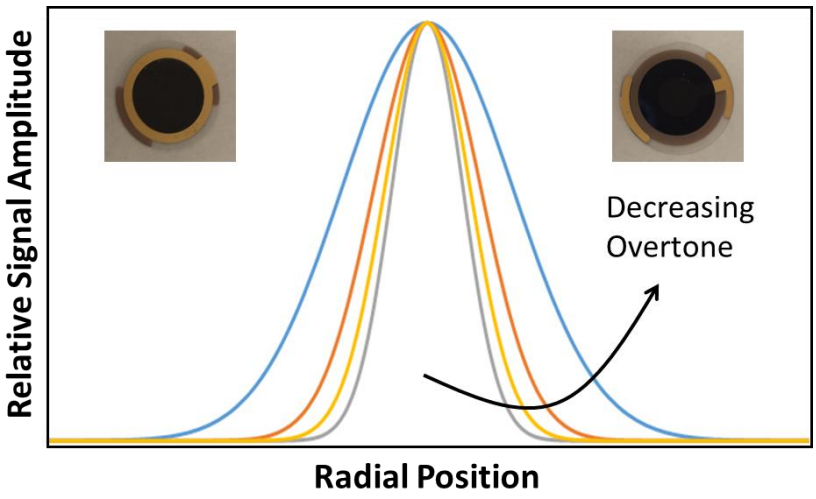

Figure 21. Sensitivity relative to the position on the quartz crystal. Adapted from Biolin Scientific by Dariya Reid.

A detailed explanation of the experimental method used in the work presented herein follows. Poly(diallyldimethylammonium chloride) (PDAC, M_w = 200,000 – 350,000 g/mol, 20 wt% solution), poly(styrene sulfonate sodium salt) (PSS, M_w = 500,000 g/mol) and linear polyethylenimine (PEI, M_w = 25,000 g/mol) were purchased from Sigma Aldrich, Scientific Polymer Products and Polysciences, Inc., respectively. QCM-D measurements were collected using the Q-Sense E1 instrument. Gold-plated AT-cut quartz crystals with a resonant frequency of 4.95 MHz were used as the substrate. Prior to film deposition the crystals were cleaned by plasma treatment using an O_2-plasma etcher for 10 min followed by a 10 min immersion in basic piranha (water (5): NH_4OH (1): H_2O_2 (1) by volume) at 70 ^oC, drying using nitrogen, and then plasma-treating for an additional 10 min. For the duration of the experiment the temperature was set to 25 ^oC and the flow rate was kept constant at approximately 115 μL/min. A zero-baseline was established by flowing Milli-Q water (pH 4.5) over the sensor for approximately 30 min. A baselayer was then deposited by passing 1 mg/mL PEI solution (pH 4.5) over the crystal for 15 min, followed by a 5 min rinse using Milli-Q water (pH 4.5) in order to increase the initial surface charge. Layer-by-layer (LbL) deposition was carried out by sequentially flowing solutions of 0.1 mg/mL PSS (0.5 M NaCl) and 0.1 mg/mL PDAC (0.5 M NaCl) over the crystal for 15 min, with a 5 min rinse of MilliQ water (0.5 M NaCl) after each deposition. Following the assembly process, the films were sequentially exposed to solutions containing $CaCl_2$, $MgCl_2$ or Na_2SO_4 at concentrations of 0.01 M – 2 M for 1-2 hrs and 0.5 M NaCl for 1 hr in order to monitor the film's response to the presence of monovalent and divalent ions.

All of the salt solutions used in this study remained stable over the duration of the experiment. $MgCl_2$ solutions showed some precipitation at higher concentrations over time. To avoid this each solution was prepared fresh on the day of the experiment. Some preliminary work was aimed at preparing LbL assemblies in the presence of multivalent salts ($MnCl_2$ and $CaCl_2$). However, the resultant films had a very rough and sticky structure. These properties are likely due to the hygroscopic nature of the salts.

2.3: Data Modeling

2.3.1: Sauerbrey Model

In order to model the frequency and dissipation data and obtain the desired parameters, a number of assumptions must be made. First of which is that the adsorbed film has a uniform thickness over the crystal area. The Sauerbrey equation is valid for flat and rigid films, $\Delta D \approx 0$, the movement of which is directly linked to the motion of the crystal; changes in frequency can be converted to changes in mass and thickness (assuming a material density) using the following linear function:[66]

$$\Delta m = -C\frac{\Delta f}{n}$$

where C is a sensitivity constant (17.7 ng/cm^2-Hz) and n is the overtone number (n = 1, 3, 5, 7, 9, 11, 13).

2.3.2: Viscoelastic Model

Films that are viscoelastic in nature, $\Delta D > 0$, are better fitted using the Voigt model. The model assumes that the film behaves as a viscoelastic solid which contains both elastic and viscous elements connected in parallel. Another assumption is that the film is laterally homogeneous with uniform thickness, density, viscosity, and elasticity. Figure 22 shows a force applied to a representative Voigt model and the resultant deformation. Figure 22 also highlights the viscoelastic nature of the Voigt model as observed in the signal lag of the deformation due to energy dissipation.

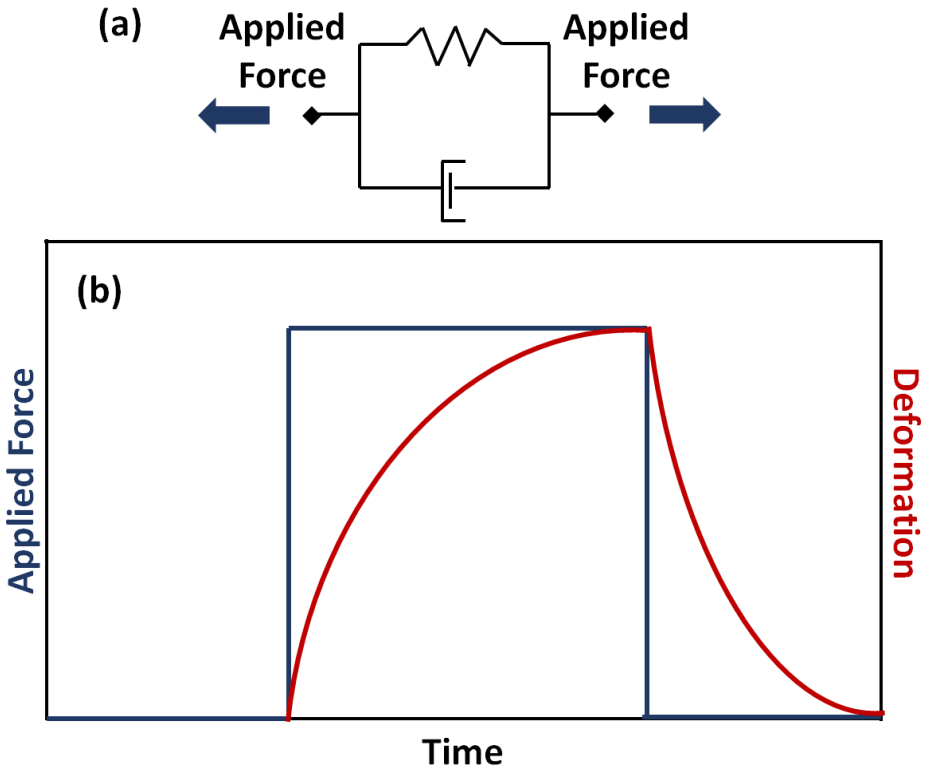

Figure 22. (a) Voigt circuit element and (b) observed deformation due to an applied force as a function of time. Adapted from Biolin Scientific by Dariya Reid.

The LbL films prepared herein are soft and viscoelastic in nature and it was found that the Sauerbrey model under-predicted film thickness. Figure 23 shows the changes in the thickness of a PDAC/PSS LbL film as it is exposed to solutions containing different ions. Figure 23 also clearly illustrates the under-predicted values of thickness obtained using the Sauerbrey model. As a result, the Voigt model was deemed more suitable to fit the data. Using the model, observed dissipation changes are broken down into the storage modulus (shear modulus) and the loss modulus (viscosity). While the frequency changes are used to determine the mass and thickness.

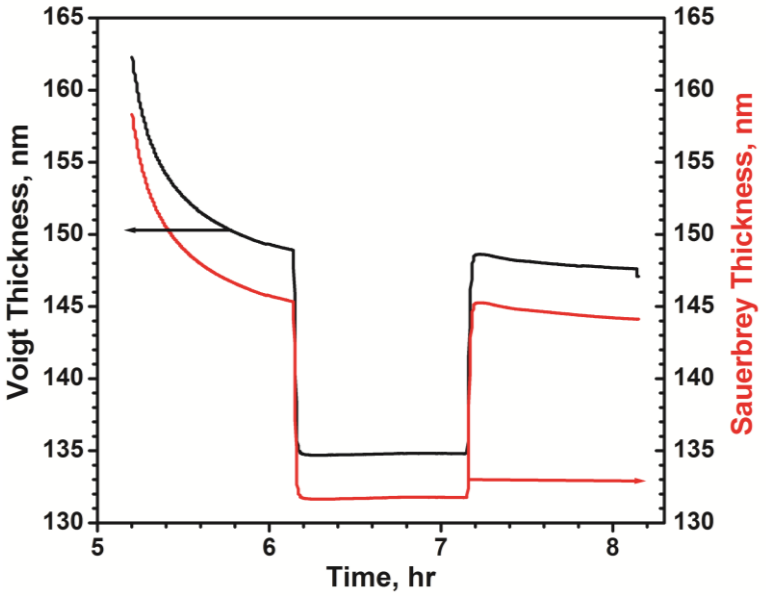

Figure 23. Observed changes in thickness of a PDAC/PSS LbL film assembled at 0.5 M NaCl as it is exposed to solutions of different ions. The raw frequency data was modeled using the Voigt model (black line) and the Sauerbrey equation (red line) to obtain the thickness values.

2.3.3: Extended Viscoelastic Model

Another important parameter to consider while modeling is the frequency dependence of the viscoelastic properties. The elastic shear modulus (*G'*) and the shear loss modulus (*G"*) of polymer solutions can be approximated using the following power law functions.

$$G' = \left(G'_0 \frac{f}{f_0}\right)^{\alpha'}$$

$$G'' = \left(G''_0 \frac{f}{f_0}\right)^{\alpha''}$$

The power law exponents α' and α'' are frequency-dependent parameters. The loss modulus can also be expressed in terms of viscosity (η) as follows.[67]

$$G"(f) = 2\pi f \eta(f)$$

Figure 24 shows the typical frequency-dependent response of a viscoelastic material. The frequency parameters α' and α'' represent the slopes of the *G'* and *G"* log-log plots, respectively. Parameter values in the range of -1 - 1 for α' and α'' values of 0 - 2 are considered reasonable for polymer solutions.[67] In the "terminal zone" α'' value is often one and suggests that the material behaves like a viscous liquid. In the "plateau zone" α'

value is close to zero and suggests that the material is primarily elastic.[67] Figure 24 also highlights the frequency range over which QCM-D operates.

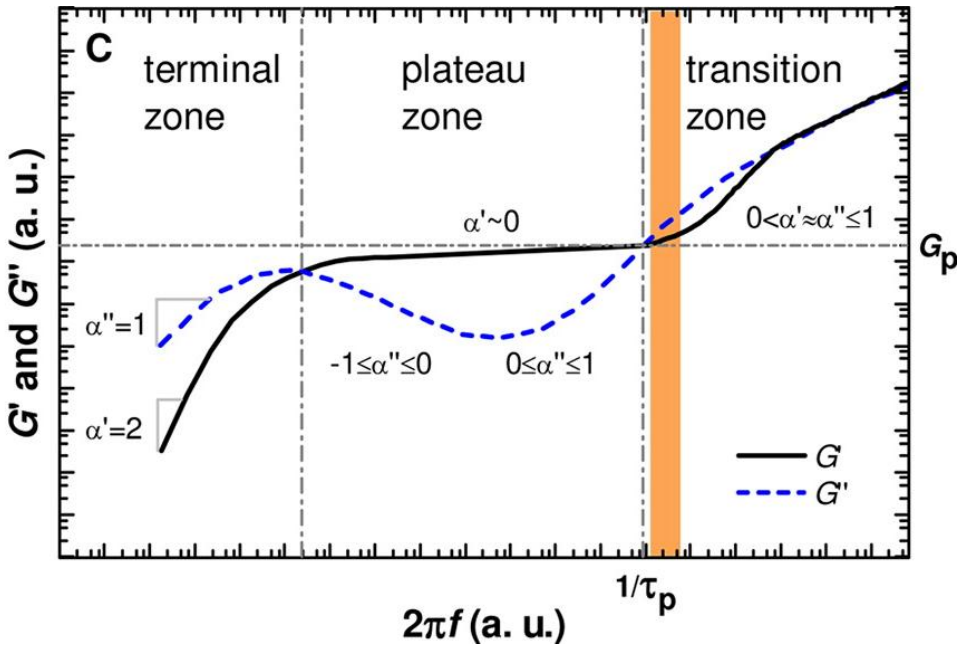

Figure 24. Frequency dependence of shear modulus and shear loss. Reprinted (adapted) with permission from Eisele, N. B.; Andersson, F. I.; Frey, S.; Richter, R. P. *Biomacromolecules* 2012, *13*, 2322-2332. Copyright 2012 American Chemical Society.

Furthermore, the extended viscoelastic model was chosen over the regular viscoelastic model as it provided a significantly lower χ^2 parameter for the data, Figure 25b. The parameters resulting from both models were close in value as is seen in Figure 25a. The QTools modeling software (Biolin Scientific) was used to fit the changes in frequency and dissipation for the 5^{th}, 7^{th} and 9^{th} overtones according to the extended viscoelastic model. Material density (L1) was taken as 1050 kg/m^3.

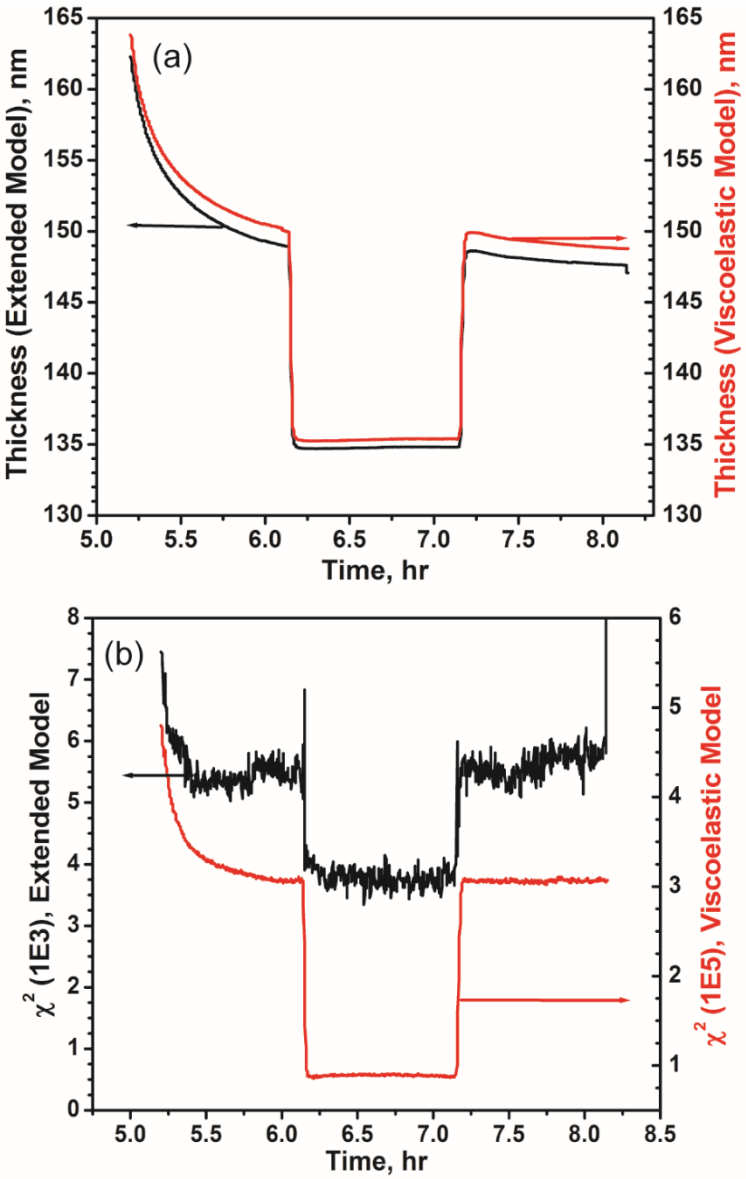

Figure 25. Observed changes in thickness and χ^2 as a function of experimental running time. The raw frequency data was modeled using the extended viscoelastic model (black line) and the viscoelastic model (red line) to obtain the thickness values and the resultant χ^2. PDAC/PSS LbL film assembled at 0.5 M NaCl.

Other models are available which predict dynamic properties of polymers. For example the "coupling model" (CM) presented by Ngai and co-workers is able to

interpret complex viscoelastic behavior which has been previously simplified by generalized rules.[68] The coupling theory presents the following arguments: 1) the relaxation of the building blocks of a polymer chain can be described using an exponential correlation function; 2) after some temperature-independent "cross-over" time the correlation function is adjusted to a stretched exponential which has an additional dependence on a coupling parameter which reflects intermolecular interactions. [68] Unfortunately, the modeling capability available for this work was limited by the QTools software.

3. MODULATED DIFFERENTIAL SCANNING CALORIMETRY OVERVIEW

Differential scanning calorimetry (DSC) monitors the amount of energy (or heat flow) necessary to maintain the temperature of a sample the same as that of a reference. In a typical experiment the heat flow is recorded as a function of temperature (for ramping measurements) or as a function of time (for isothermal measurements). A simplified schematic of the instrument is shown in Figure 26.

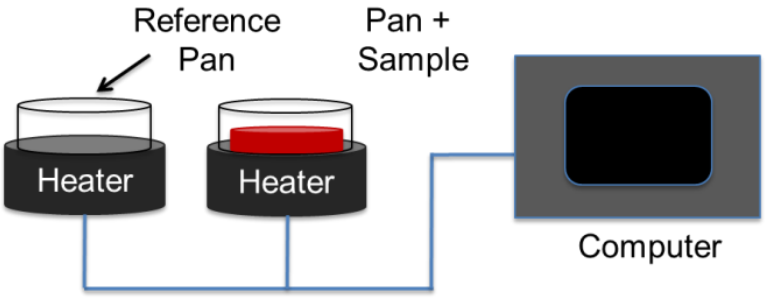

Figure 26. Schematic representation of a typical DSC set up.

Modulation is often used in the case of weak thermal transitions or when the thermal response has overlapping features and is difficult to resolve.[69] The term modulation refers to an additional sinusoidal heating rate that is overlaid in addition to the linear heating rate that is used in conventional DSC.[69] Essentially the linear heating rate is a constant value while the modulated rate is an oscillating wave of given amplitude and

period. Control over the applied amplitude and period allows the user to improve the sensitivity and the quality of the collected data.[69]

The application of these two heating rates allows the overall or the "total" heat flow data to be separated into two components.[70] The reversing component, often referred to as the "heat capacity component", reflects the segment of the heat flow which is affected by the modulations in the heating rate. As the name suggests this segment represents thermal features associated with heat capacity changes and melting.[70] The nonreversing component, often referred to as the "kinetic component", indicates the segment of the heat flow that is time-dependent and is evaluated by taking a difference of the total heat flow and the reversing heat flow.[70] The total heat can be written in terms of the variables just described in the following manner:

$$\frac{dH}{dt} = C_p \frac{dT}{dt} + f(T,t)$$

where C_p is the heat capacity of the material being tested, *dT/ dt* is the applied heating rate and *f(T,t)* is the nonreversing heat flow.[70]

As previously mentioned, one attribute of MDSC is its ability to distinguish between two thermal events occurring within the same temperature range. Figure 27 shows an example of distinguishing enthalpic relaxation from the glass transition of polycarbonate.[71] Enthalpic relaxation appears in DSC scans of glassy polymers as an endothermic peak near T_g. The feature represents changes in the thermal properties of an amorphous material below the T_g as it tends towards equilibrium.[72] Because enthalpic

relaxation is a time-dependent process the nonreversing signal is able to capture this thermal feature. While the reversing signal is able to clearly resolve the glass transition.[73]

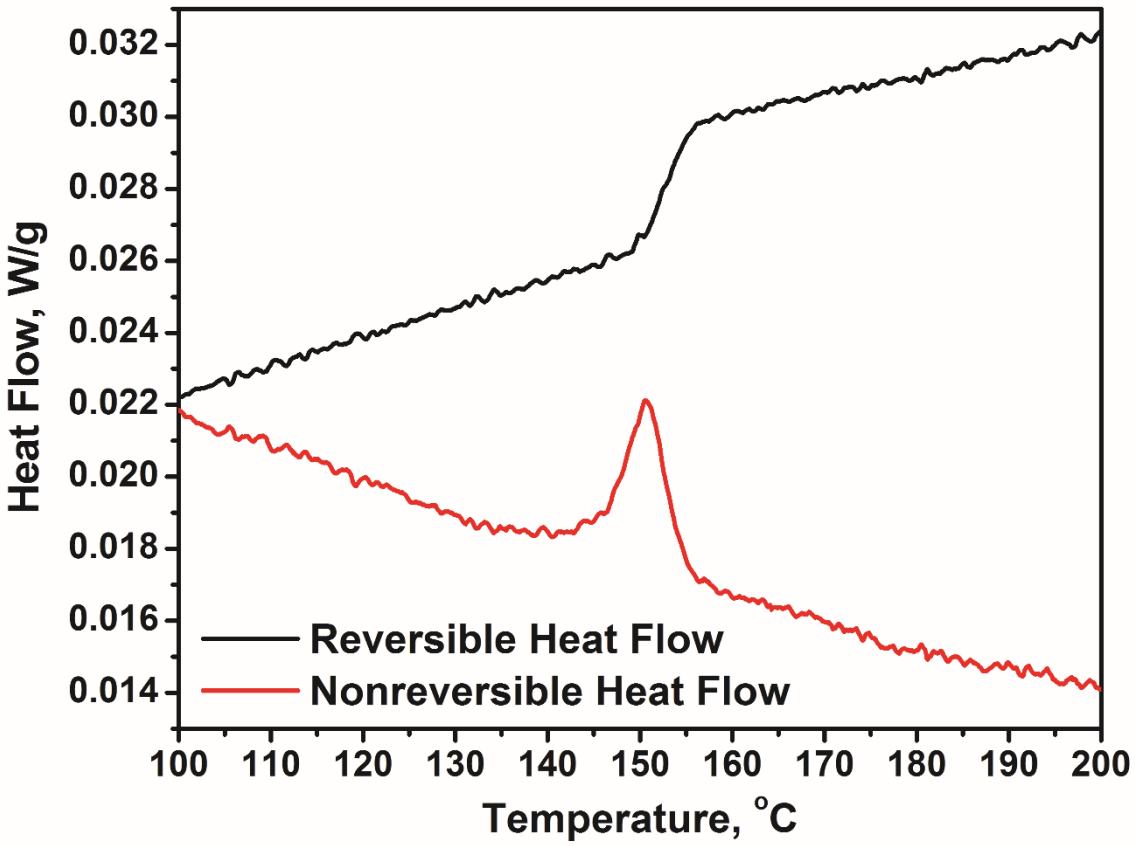

Figure 27. Thermal response of a polystyrene sample throughout an aging process. Reprinted (adapted) with permission from Reid, D. K.; Alves Freire, M.; Yao, H.; Sue, H.-J.; Lutkenhaus, J. L. *ACS Macro Letters* 2015, *4*, 151-154. Copyright 2015 American Chemical Society.

In order to improve the sensitivity of the experiment and the resolution of the collected data some key input parameters (modulation period and amplitude, average

heating rate) must be optimized. The modulation period must allow enough time for the thermal energy to transfer between the stage and the sample but be kept within a reasonable experimental running time.[74] Modulation amplitude must also be chosen as a tradeoff between two competing effects. Increasing modulation amplitudes improves the sensitivity.[74] However, overly high amplitudes result in lower resolution. The heating rate must then be chosen based on the selected modulation period and amplitude.[74] TA Instruments provides some excellent guidelines in choosing these parameters.

4. RESULTS – STRUCTURAL AND MECHANICAL RESPONSE

4.1: General Structural Behavior

A recent study presented by Wei *et al*. explored the effect of divalent cation solutions on the properties of poly(diallyldimethylammonium chloride) (PDAC) / poly(styrene sulfonate) (PSS) polyelectrolyte multilayers (PEM).[75] Researchers showed that ultra-thin PDAC/PSS films, with PSS as the terminating layer, assembled from monovalent salt solutions and then equilibrated with water or the rinsing solution contracted due to physical crosslinking when exposed to divalent cation solutions of low concentration.[75] Physical crosslinking was shown to be reversible when the films were equilibrated with monovalent solution but not when deionized water was used. At greater divalent salt concentrations an expansion of the PEM was observed due to the penetration of the counterions and the associated water molecules into the film.[75] The effect of divalent anions and a detailed concentration dependency remains relatively unexplored.

The work presented herein focuses on the swelling of poly(ethylene imine) (PEI)-(PSS/PDAC) multilayers when in the presence of divalent counterions (both anions and cations). The effect is investigated as a function of concentration and the differences in the behavior between cations and anions are explained in terms of osmotic pressure and Donnan exclusion principle. The effects are measured using quartz crystal

microbalance with dissipation (QCM-D) and modulated differential scanning calorimetry (MDSC).

Figure 28 illustrates the layer-by-layer (LbL) assembly process of a PEM as monitored by QCM-D. The experimental details are described in section 2.2. The observed changes in frequency and dissipation are due to the deposition of the prelayer of PEI and then the sequential adsorption of PSS and PDAC. The reduction in frequency indicates uptake of mass and increase in thickness as more layers are deposited. The step changes start out equal for the deposition of PSS and PDAC. However, at higher layer pair number the deposition of PDAC presents as a significantly larger frequency change as compared to PSS. This feature may be due to a larger extent of penetration of the PDAC chain into the bulk of the film. The film is built up to seven bilayers and the ionic strength of all solutions during build up is kept constant at 0.5 M NaCl. The observed dissipation changes oscillate at a constant value. Similar to the frequency response at larger layer pair number the increase in dissipation is larger during the deposition of PDAC relative to PSS.

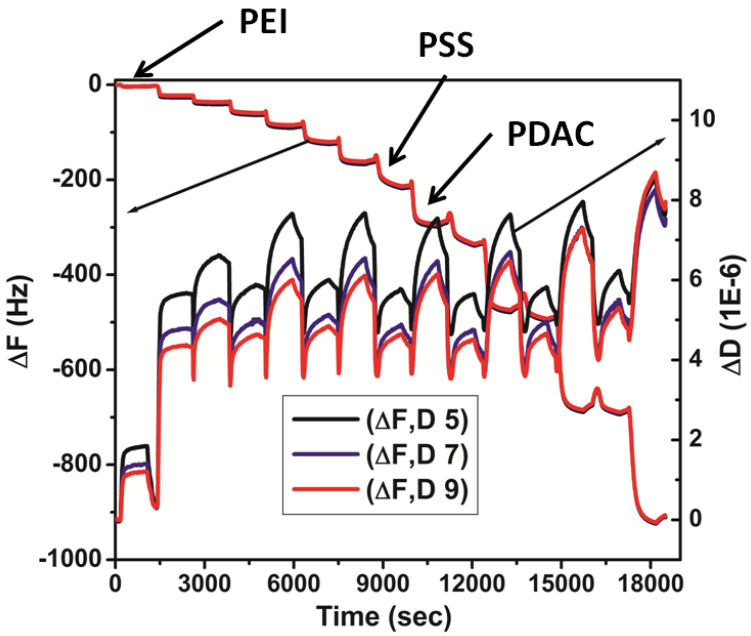

Figure 28. Changes in frequency and dissipation collected by QCM-D during the LbL assembly process of a PDAC/PSS film.

Once the assembly process is completed the LbL film was first exposed to varying concentrations of NaCl in order to establish the effect of concentration prior to investigating the effect of ion type. As is displayed in Figure 29a the structure of the exposed film responded to the changes in solution when the ionic strength was drastically higher or lower compared to the solution used during film build-up (0.5 M NaCl) but not for the intermediate concentrations. When the contact solution was changed from 0.01 M NaCl to 0.5 M NaCl the film contracted by 189 nm. Alternately, when the solutions were reverted back from 0.5 M NaCl to 0.01 M NaCl the film expanded by 86 nm. The response was similar when the film was subject to 1 M and 2 M NaCl solution exchange; first the film contracted by 13 nm and 75 nm, then expanded by

12 nm and 67 nm, respectively. Changing the contact solution from 0.5 M to 1/6 M or 1/3 M NaCl produced insignificant changes in the film thickness response. The magnitude of contraction at different concentrations of NaCl can be viewed more clearly in Figure 29b. Due to the stark difference in response of the LbL film exposed to solutions of low and high ionic strength, from this point on in the report the ion concentration range studied will be segmented into two parts.

- Regime I: Concentrations below 1/6 M
- Regime II: Concentrations above and including 1/6 M

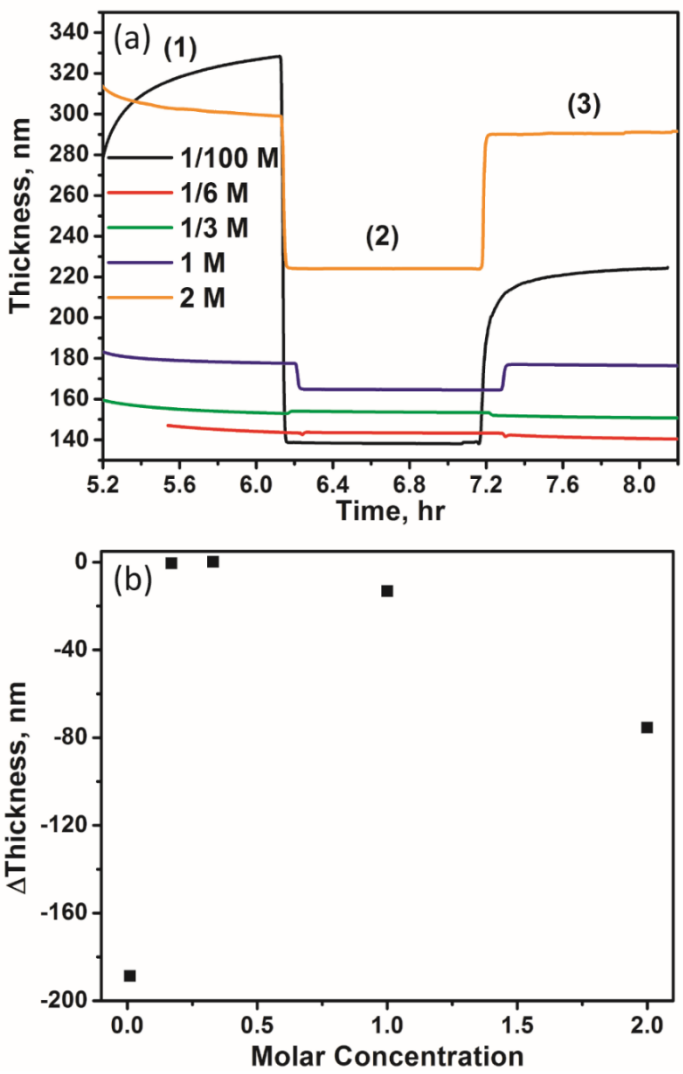

Figure 29. (a) Observed changes in thickness as a function of time for an LbL film exposed to solutions of NaCl of varying concentrations. The numerals mark exposure to NaCl solutions of changing concentration [(1) and (3)] and 0.5 M NaCl solution [(2)]. The data was shifted along the y-axis for clarity of presentation. (b) Change in thickness as a function of NaCl concentration.

In this work the primary focus is to study the response of PDAC/PSS multilayers to ion solutions of varying valency. Table 1 lists a collection of ions, which were considered for this study along with some common properties that relate to ion-water interactions. It was desirable to work with ions which differ significantly in properties

such as viscosity coefficient and hydration number from Na^+ and Cl^-, which are present during the build-up of the film. As such, Ca^{2+}, Mg^{2+} and SO_4^{2-} were chosen as ions of interest. The ions were used as sodium and chloride salts in order to keep the corresponding anion or cation constant relative to NaCl.

Table 1. Properties of various ions.

Ions	**Viscosity Coefficient[76]**	**Hydration Number[77]**	**$\Delta_{hyd}G$[77] (kJ/mol)**
Mg^{2+}	0.385	10	-1830
Ca^{2+}	0.285	7.2	-1505
Ba^{2+}	0.22	5.3	-1250
Li^+	0.150	5.2	-475
Na^+	0.086	3.5	-365
K^+	-0.007	2.6	-295
NH_4^+	-0.007	2.4	-285
PO_4^{3-}	0.590	4.5	-2765
SO_4^{2-}	0.208	3.1	-1080
$CH_3CO_2^-$	0.250	2.2	-365
F^-	0.10	2.7	-465
HCO_2^-	0.052	2.1	-395
Cl^-	-0.007	2.0	-340
Br^-	-0.032	1.8	-315

In order to investigate the effect of ion type on the structure of an LbL film, PDAC/PSS multilayers were first deposited onto a QCM-D crystal from 0.5 M NaCl solutions. Following film deposition, changes in frequency and dissipation were monitored as the LbL film was exposed to particular salt solutions. The switching of solutions occurred once a plateau in the signal was reached. Figure 30 shows the observed changes in frequency and dissipation upon ion exchange. Following the notation of Figure 30 the experimental steps are summarized as follows:

(1) Solutions of divalent salts (0.01 M – 2 M) are flown over the films

(2) Solution of 0.5 M NaCl is flown over the film

(3) Repeat step (1)

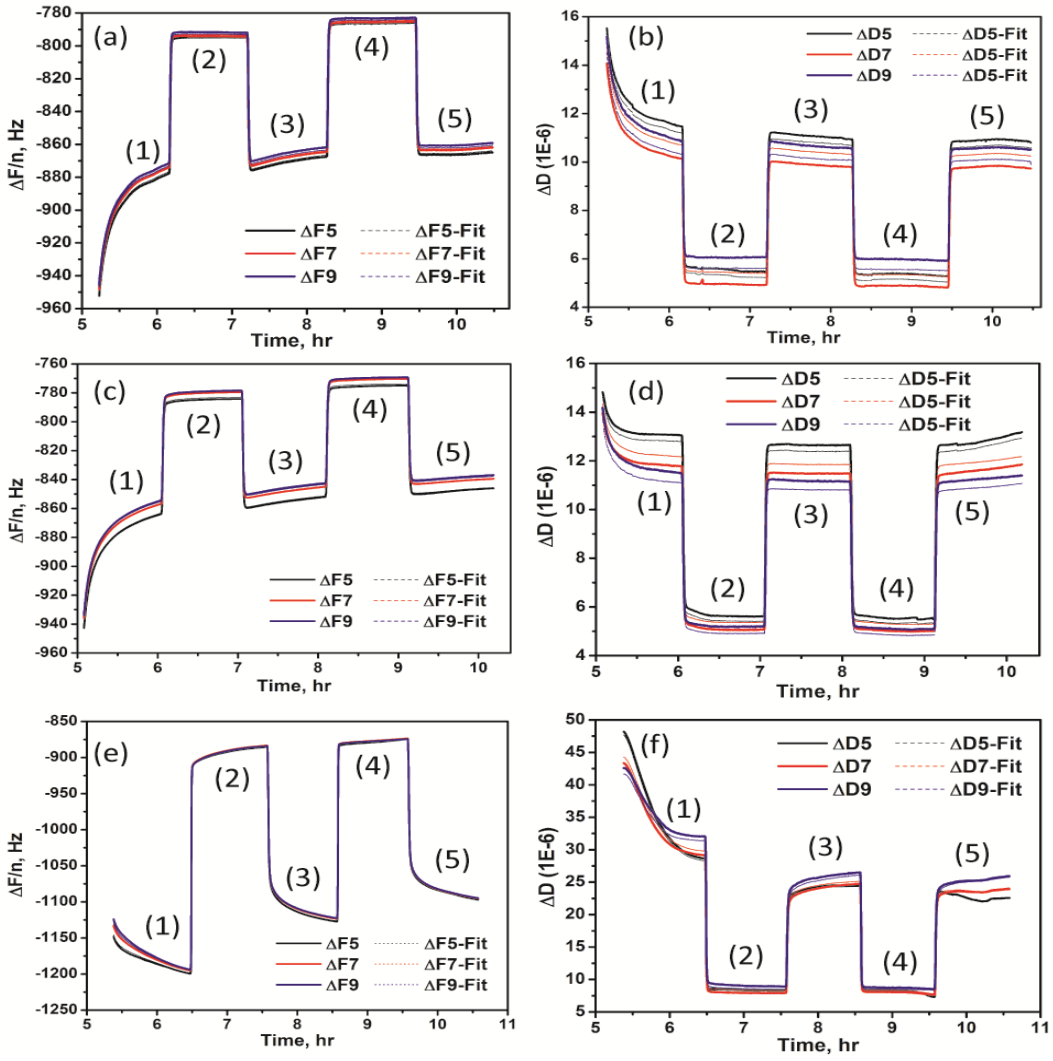

Figure 30. Response of a PEI-$(PSS/PDAC)_7$ LbL multilayer film to repeated exposure of divalent and monovalent salt solutions. Normalized frequency changes collected by QCM-D upon contact of an LbL film with (a) 1/3 M $CaCl_2$, (c) 1/3 M $MgCl_2$ and (e) 1/3 M Na_2SO_4. Changes in dissipation upon introduction of (b) 1/3 M $CaCl_2$, (d) 1/3 M $MgCl_2$ and (f) 1/3 M Na_2SO_4. Solid lines indicate raw data. Dashed lines indicate the fit provided by QTools software. Data for the 5^{th}, 7^{th} and 9^{th} overtones are shown. The numerals (1), (3) and (5) mark exposure to divalent salt solutions and numerals (2) and (4) mark exposure to 0.5 M NaCl solution.

An increase in the frequency, step up from (1) to (2), was observed as the flowing solution was switched from 1/3 M $CaCl_2$ to 0.5 M NaCl, Figure 30a. This step change indicates a reduction in the thickness of the film and the amount of adsorbed mass interacting with the QCM-D crystal. The change is also mirrored by a sharp reduction in dissipation indicating that the LbL film is more compressed and rigid, Figure 30b. A subsequent reduction in frequency, step down from (2) to (3), was observed when the flowing solution was switched back from 0.5 M NaCl to 1/3 M $CaCl_2$. The reversal in frequency illustrates an expansion of the film and uptake of mass, Figure 30a. Similarly, the change in dissipation nearly recovers its previous value illustrating that the film is softer, Figure 30b. Figure 30 shows that this step change switching phenomena is shown to be repeatable within the same sample. The film displayed nearly identical behavior when exposed to solutions of 1/3 M $MgCl_2$. The described changes were also observed for films exposed to 1/3 M Na_2SO_4 solutions with alike trends but increased magnitude of change, Figure 30e-f. However, it is important to note that the larger magnitude of response observed in Na_2SO_4 is not true for all concentrations. As seen in Figure 30, there is a strong overlay of the solid and dashed lines indicating a good fit of the predicted model and the raw data. χ^2 provides a quantifiable measure of the goodness of fit for the model and the parameters used to convert the raw QCM-D data to obtainable viscoelastic properties of the material. The extended viscoelastic model was chosen to treat the raw data due to the reduced χ^2 values.

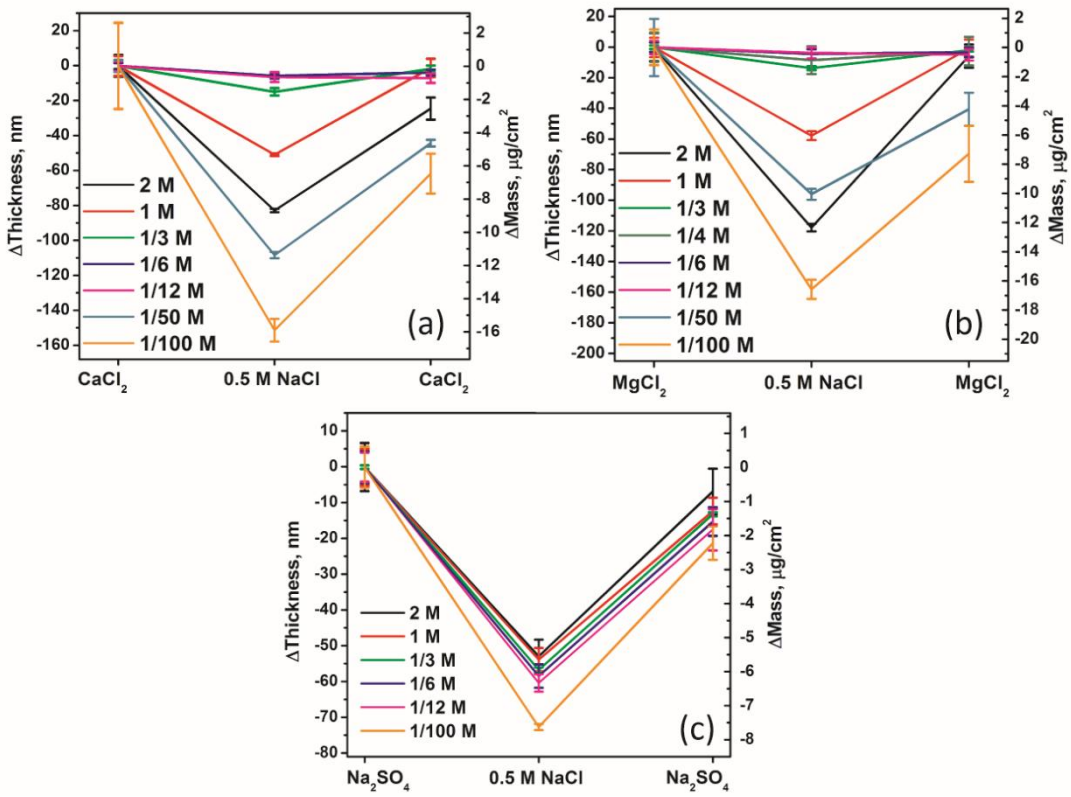

Figure 31. Mass and thickness changes averaged over ten minutes of exposure to varying concentrations of (a) $CaCl_2$, (b) $MgCl_2$ and (c) Na_2SO_4. Data was used from the region of the step in which ΔF and ΔD changed by less than 0.025 and 0.885%, respectively, over the course of ten minutes. Error bars represent the standard deviation over three samples.

Data shown in Figure 30 was collected for ion exchange with 0.5 M NaCl over a series of concentrations of $CaCl_2$, $MgCl_2$ and Na_2SO_4 solutions. This data was re-plotted in Figure 31 to determine any observable dependence of the thickness and mass changes with respect to the concentration of divalent salts in contact with the LbL film. Figure 31a - b shows that in the case of $CaCl_2$ and $MgCl_2$ exposure the magnitude of the expansion and contraction of the film increases with increasing concentration in Regime II. However in Regime I the step change becomes larger as the concentration decreases.

The reported change in thickness is negative, *i.e.* the film is contracting, when the solution is switched from divalent salt solution to 0.5 M NaCl. While, when the solution is switched from 0.5 M NaCl to $CaCl_2$ or $MgCl_2$ the film expands, *i.e.* the change in thickness is positive. Similar analysis was carried out on films exposed to Na_2SO_4 solutions. However, Figure 31c shows that the data sets for different concentrations partially overlap with no distinguishable dependence on the concentration. The change in thickness is still observed as negative when the solutions are switched from Na_2SO_4 to 0.5 M NaCl and positive when 0.5 M NaCl is replaced with Na_2SO_4.

4.1.1: Concentration Dependence

As previously stated, increasing the concentration of the $CaCl_2$ and $MgCl_2$ solutions in contact with the PDAC/PSS multilayer past a certain threshold (Regime II) results in a parallel increase in the amount of contraction or expansion experienced by the film. In fact, Figure 32a-b shows that the change in thickness increases linearly with the concentration. The resultant values can be fitted using $\Delta h = -43.26C_{CaCl2} + 0.20$ (R^2 = 0.98) and $\Delta h = -62.48C_{MgCl2} + 6.48$ (R^2 = 0.99) for Regime II concentrations of $CaCl_2$ and $MgCl_2$, respectively. The magnitude of the structural change observed in Regime II is larger for $MgCl_2$ as compared to $CaCl_2$ ion exchange. In Regime I the identity of the ion does not affect the resultant thickness change. The maximum contraction observed when switching contact solutions from divalent salt to 0.5 M NaCl is approximately 160 nm for 0.01 M $CaCl_2$ and $MgCl_2$ solutions. In the case of Na_2SO_4 exposure the change in

thickness quickly reaches a plateau and the amount of contraction or expansion experienced by the film remains constant regardless of the salt concentration.

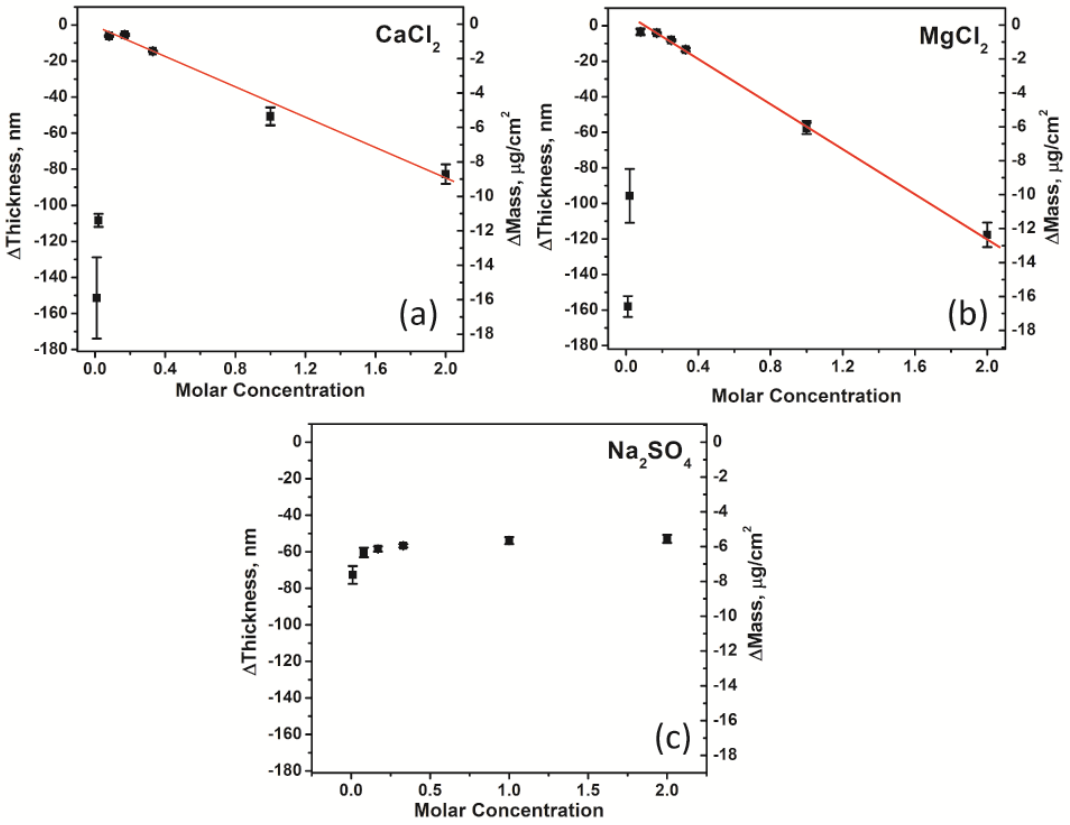

Figure 32. Concentration dependence of the thickness and mass changes of LbL multilayer films when exposed to multivalent ion solutions. Net change in thickness observed during the ion exchange from (a) $CaCl_2$, (b) $MgCl_2$ and (c) Na_2SO_4 to 0.5 M NaCl. The solid lines are drawn to help guide the eye and represent a linear fit of $\Delta h = -43.26C_M + 0.20$ ($R^2 = 0.98$) and $\Delta h = -62.48C_M + 6.48$ ($R^2 = 0.99$) for exchange from $CaCl_2$ and $MgCl_2$, respectively to 0.5 M NaCl.

Table 2 summarizes the parameters obtained from the linear fits of the NaCl, $CaCl_2$ and $MgCl_2$ data in Regime II as well as the hydration numbers for the ions

handled in this study. The increased slope observed for $MgCl_2$ as compared to $CaCl_2$ potentially indicates two things: 1) Mg^{2+} is a superior doping agent as compared to Ca^{2+} therefore at the same molar concentration more Mg^{2+} ions penetrate the film and cause a greater degree of expansion; 2) because Mg^{2+} has a larger hydration shell as compared to Ca^{2+} more water molecules enter the film during doping, causing greater expansion.

Table 2. Summary of fitted parameters.

Ions	**Hydration Number**[78]	**Slope**	**Y-intercept**	**R^2**
Na^+	3.5	N/A	N/A	N/A
Cl^-	2.0	N/A	N/A	N/A
Ca^{2+}	7.2	N/A	N/A	N/A
Mg^{2+}	10	N/A	N/A	N/A
SO_4^{2-}	3.1	N/A	N/A	N/A
NaCl	N/A	-41.56	14.10	0.92
$CaCl_2$	N/A	-43.26	0.20	0.98
$MgCl_2$	N/A	-62.94	6.52	0.99

4.2: Mechanical Properties

Figure 33 provides the shear modulus values as a function exposure time to divalent and monovalent salt solutions, as labeled in the figure. Due to the low $\Delta F/\Delta D$ ratio the QTools software had difficulty providing an acceptable fit of the viscoelastic parameters. The resultant data was often noisy and inconsistent with the original trend in frequency and dissipation. The full range of shear modulus values shown are averaged values taken from two to three separate samples over a similar time range. Although the values of shear modulus presented should not be taken as absolute due to the uncertainty presented by the model; the trend evident in the data can be used to state a couple of conclusions. The observed increase in the shear modulus of the material suggests that the LbL films become stiffer when exposed to NaCl as compared to when in the presence of divalent ions. The step change increase in the shear modulus ranges from less than 1 MPa for 1/6 M $CaCl_2$ to about 11 MPa for 0.01 M $CaCl_2$. The magnitude of the change in shear modulus is highest at the lowest ion concentrations for all three investigated salts. Figure 33 shows that when the exposure solution was switched from 0.01 M $CaCl_2$ to 0.5 M NaCl the shear modulus increased by 11 MPa. When the solutions were switched back the shear modulus dropped by 10 MPa. Similarly the shear modulus increased by 10 MPa when the exposure solution was switched from both 0.01 M $MgCl_2$ and 0.01 M Na_2SO_4 to 0.5 M NaCl. The modulus response then recovered by 8 MPa when the solutions were switched back.

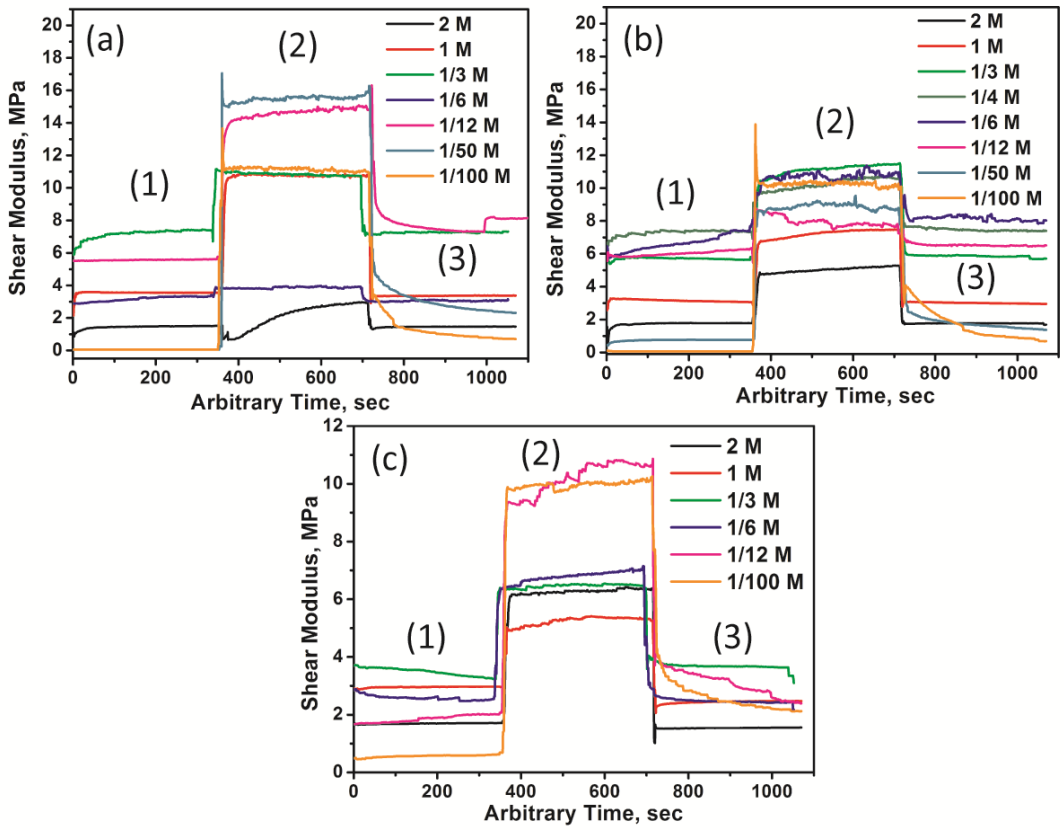

Figure 33. Changes in viscoelastic properties of PEI-$(PSS/PDAC)_7$ upon ion exchange. Shear modulus as a function of exposure time is shown for a range of concentrations of (a) $CaCl_2$, (b) $MgCl_2$ and (c) Na_2SO_4. The numerals mark exposure to $CaCl_2$, $MgCl_2$ or Na_2SO_4 solution [(1) and (3)] and 0.5 M NaCl solution(2).

4.3: Film Thickness Dependence

Figure 34 shows the relative and the percent change in film thickness of LbL films of varying layer pair number prepared from 0.5 M NaCl solutions upon exposure to 0.01 M $CaCl_2$ and 1/6 M $CaCl_2$. These two concentrations were chosen in order to probe the overall thickness effect in both Regime I and Regime II. As is evident from the graphs, the change in thickness as the polyelectrolyte multilayer is undergoing ion exchange increases as the overall thickness of the film increases. This behavior is

observed upon exposure of the LbL film to both 0.01 M $CaCl_2$ (Figure 34a) and 1/6 M $CaCl_2$ (Figure 34b). Percent change presents differently. Figure 34a and 34b show no apparent trend in percent change with respect to layer pair number. These observations indicate that the contraction and expansion of the film upon ion exchange occurs uniformly along the full depth of film. Conversely, if contraction/expansion occurred in a fixed volume, the percent change would decrease as the number of layer pairs increased, which is contrary to our observations.

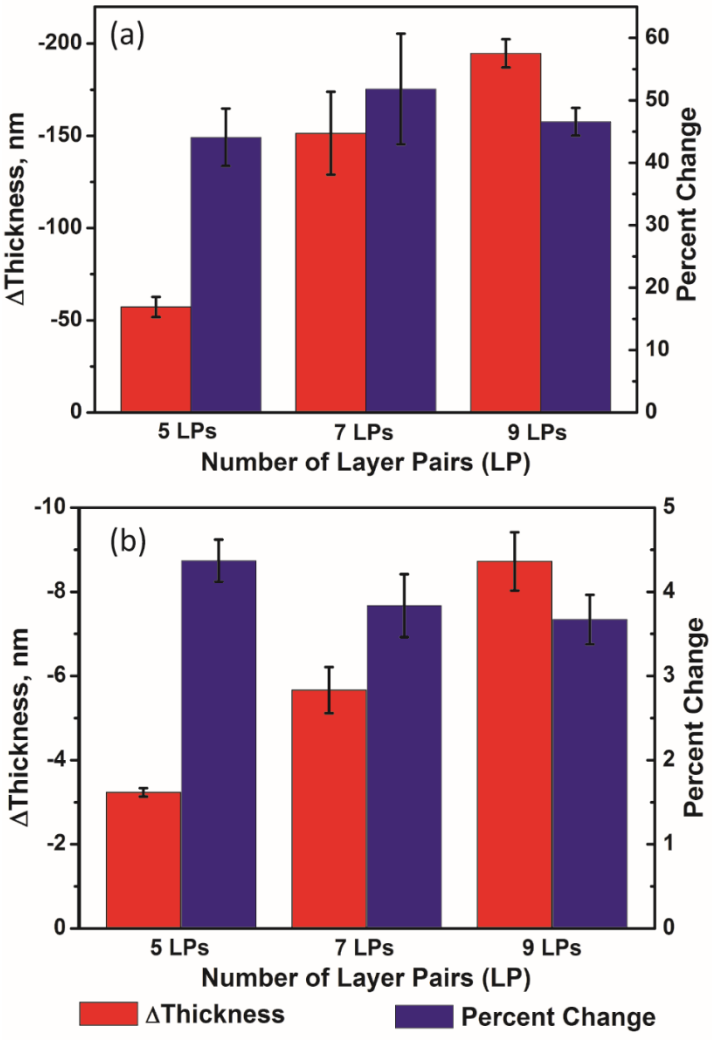

Figure 34. Effect of overall film thickness on the response of PEI-$(PSS/PDAC)_x$ LbL films to ion exchange. The error bars represent the standard deviation taken from an average of three samples. All samples were built-up from 0.5 M NaCl up to the designated number of layer pairs and then sequentially exposed to ion solutions. Change in thickness and percent change in thickness upon contraction due to solution switch from (a) 0.01 M $CaCl_2$ to 0.5 M NaCl and (b) 1/6 M $CaCl_2$ to 0.5 M NaCl as a function of layer pair number are shown.

4.4: Discussion

4.4.1: Structural Changes

The swelling of polyelectrolyte multilayers is not a new phenomenon. LbL assemblies have been previously shown to swell due to the presence of ionic liquids[43] and changes in ionic strength,[40] to name a few. The swelling of PEI-(PSS/ poly(allylamine hydrochloride) $(PAH)_4$-PSS and PEI-$(PSS/PDAC)_4$-PSS was observed using QCM-D when in the presence of ionic liquid (IL)/water mixtures.[43] As shown in Figure 35 both of the multilayer systems displayed increasing degree of swelling when exposed to progressively higher concentrations of IL. The cut off concentrations for each system represent the upper concentration limit beyond which the LbL film began to decompose.[43] The researchers also found that at a given concentration the combination of the more hydrophobic polyelectrolyte pair (PDAC/PSS) and the more hydrophobic IL resulted in the maximum degree of swelling.[43]

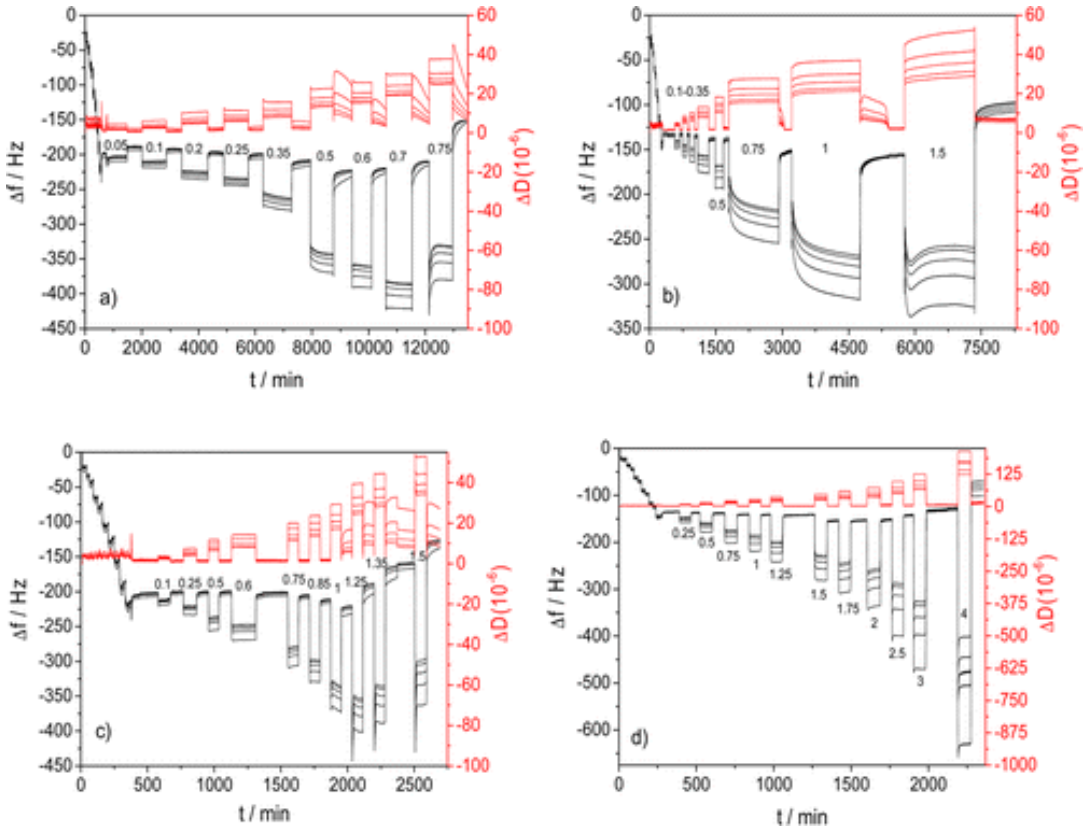

Figure 35. Changes in frequency and dissipation observed for (a) PEI-$(PSS/PDAC)_4$-PSS exposed to 1-hexyl-3-methylimidazolium chloride (HMIM), (b) PEI-$(PSS/PAH)_4$-PSS exposed to HMIM, (c) PEI-$(PSS/PDAC)_4$-PSS exposed to 1-methyl-3-methylimidazolium chloride (EMIM) and (d) PEI-$(PSS/PAH)_4$-PSS exposed to EMIM. The numerals indicate the concentration of IL at each step change. Reprinted (adapted) with permission from Parveen, N.; Schönhoff, M. *Macromolecules* 2013, *46*, 7880-7888. Copyright 2013 American Chemical Society.

Hydrophobicity was also demonstrated to play a role in the swelling of LbL assemblies exposed to salt solutions of varying ionic strength. Figure 36 shows that increased hydrophobicity of the polyelectrolyte pair led to a decreased degree of swelling when PSS / poly(acrylic acid) (PAA), PSS/PDAC and PSS/PAH LbL films were compared.[40] The hydrophobic nature of the polyelectrolyte pair indicates that the polymer chains

would rather interact with each other rather than with the surrounding water molecules. As a result these films don't show a considerable degree of swelling as compared to other polyelectrolyte pairs due to unfavorable interactions with water.[40]

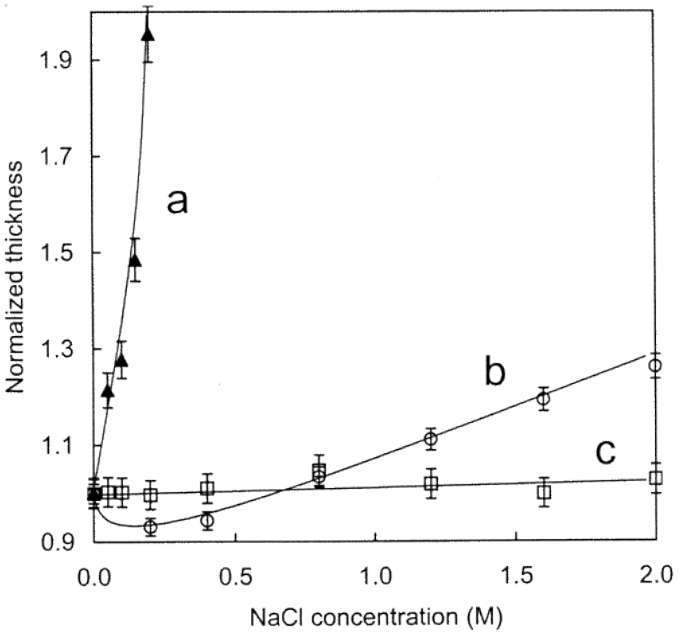

Figure 36. Swollen thickness normalized by the thickness of the dry film as a function of salt concentration for PAA/PDAC (a), PSS/PDAC (b) and PSS/PAH (c) LbL films. Measurements were collected using AFM. Reprinted (adapted) with permission from Dubas, S. T.; Schlenoff, J. B. *Langmuir* 2001, *17*, 7725-7727. Copyright 2001 American Chemical Society.

The data presented herein shows that the primary response of the LbL films occurs upon exposure to divalent salts; thus, the interaction of the divalent ions with the polyelectrolyte chains is of great importance. Divalent ions, in theory, could cause bridging, a form of physical crosslinking, between the polyelectrolyte chains as has been seen in a number of polyelectrolyte multilayer systems. As can be seen in Figure 37 a

metal−ligand complex was formed between branched-PEI and a collection of divalent metal ions which was then used to prepare LbL films with PAA as the polyanion. These multilayers were shown to controllably degrade under certain pH conditions through the formation of pores within the structure of the film.[79] The observed color change in the LbL film was used as indication of the formation of the metal complex. The presence of the metal ions also caused stiffening of the film as indicated by increasing Young's modulus and hardness.[79]

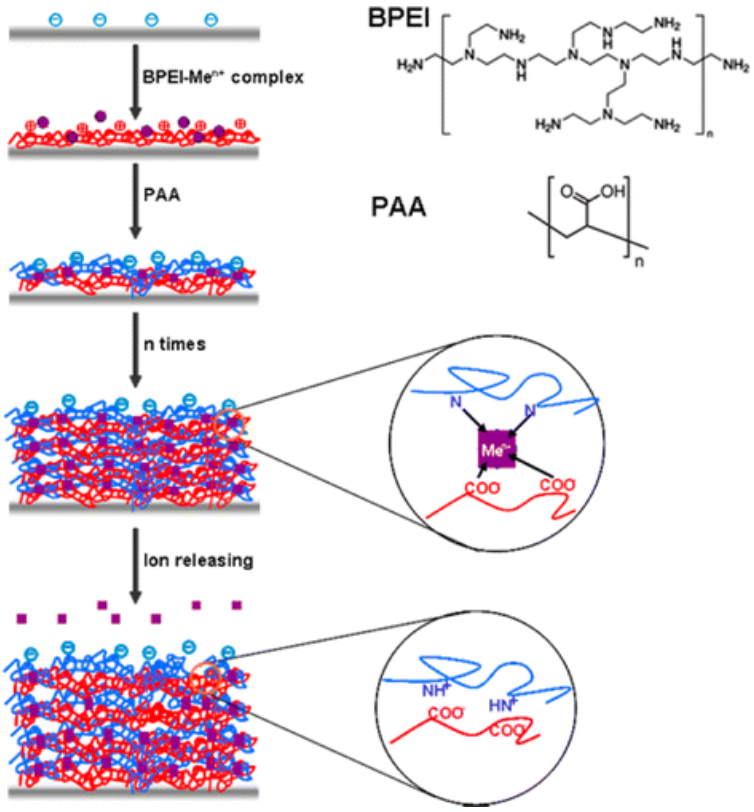

Figure 37. Schematic representation of the formation of BPEI/PAA LbL films containing BPEI-metal complex. Reprinted (adapted) with permission from Huang, X.; Schubert, A. B.; Chrisman, J. D.; Zacharia, N. S. *Langmuir* 2013, *29*, 12959-12968. Copyright 2013 American Chemical Society.

Metal−ligand coordination was also achieved for PSS/poly(4-vinyl pyridine) (P4VP) LbL assemblies in the presence of both copper[80] and cobalt.[81] However, such complexation is unlikely for the polyelectrolyte system in this work as this would cause a contraction of the films in the presence of divalent ions, as is seen in the case of poly(methacrylic acid) (PMAA) brushes in the presence of metal ions, instead the reverse is observed.[82] Figure 38 illustrates a reduction in polyelectrolyte brush thickness with increasing concentration of both $Ca(NO_3)_2$ and $Al(NO_3)_3$. The collapse of the brushes is attributed to bridging in the case of Al^{3+} exposure and reduction in the hydrophobicity of the polyelectrolyte brush with greater presence of Ca^{2+} ions.[82]

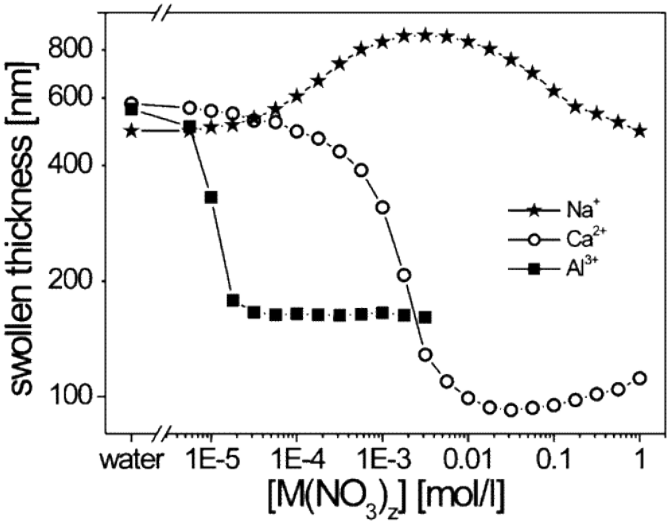

Figure 38. Swollen thickness of a PMAA brushes as a function of solution concentration. Reprinted (adapted) with permission from Konradi, R.; Rühe, J. *Macromolecules* 2005, *38*, 4345-4354. Copyright 2005 American Chemical Society.

In brief summary, the structural changes observed are expansion of the LbL film upon exposure to divalent salt solutions and contraction of the film upon exposure to monovalent salt solutions. A possible reason for the changes in thickness of the films can be found by comparing the hydration shells of the ions the films are exposed to. Divalent ions have a significantly larger hydration shell as compared to the monovalent ions. For example in literature the hydration number for calcium is about 9[83-84] and for sodium it is about 4[85] at room temperature. As is illustrated in Figure 39 the observed change in thickness can be attributed to the associated water molecules entering and leaving the film.

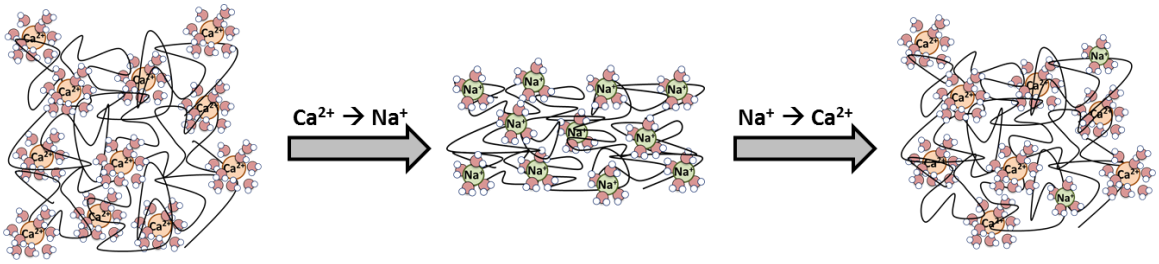

Figure 39. Schematic representation of the contraction and expansion of an LbL film during ion exchange.

Relative hydration of each component in the examined system can take on the form of the following balanced equation for ion doping with a multivalent cation:[86]

$$n[Pol^{+}Pol^{-} \bullet xH_2O] + C^{n+} \bullet aH_2O_{aq} + n[A^{-} \bullet bH_2O_{aq}] \rightleftharpoons n[Pol^{+}A^{-} \bullet cH_2O] + Pol_n^{-}C^{n+} \bullet dH_2O + yH_2O_{aq}$$

and anion:

$$n[Pol^{+}Pol^{-} \bullet xH_2O] + A^{n-} \bullet eH_2O_{aq} + n[C^{+} \bullet fH_2O_{aq}] \rightleftharpoons Pol_n{}^{+}A^{n-} \bullet gH_2O + n[Pol^{-}C^{+} \bullet hH_2O] + yH_2O_{aq}$$

where Pol^{+} and Pol^{-} are the polycation and polyanion chains, respectively; C^{n+} and C^{+} are the multivalent and monovalent cations, respectively; A^{n-} and A^{-} are the multivalent and monovalent anions, respectively; a and f are the water molecules associated with the multivalent and monovalent cations in solution, respectively; b and e are the water molecules associated with the monovalent and multivalent anions in solution, respectively; c, d, g and h are the waters associated with the respective extrinsic ion pairs; x is the number of water molecules hydrating the intrinsically compensated sites and y represents the remaining water molecules.[86]

The major difference observed in the swelling behavior at low and high ionic concentrations of divalent cation solutions ($CaCl_2$ and $MgCl_2$) has been previously observed using Fourier transform infrared spectroscopy (FTIR) in PSS-terminated PDAC/PSS multilayers.[86] Using FTIR spectra researchers were able to determine the molar fraction of water molecules in the film relative to the sulfonate groups for a series of concentrations and a collection of ions. Figure 40 reveals that the resultant data revealed a trend that mirrors the relationship obtained using QCM-D when analyzed as a function of concentration.[86]

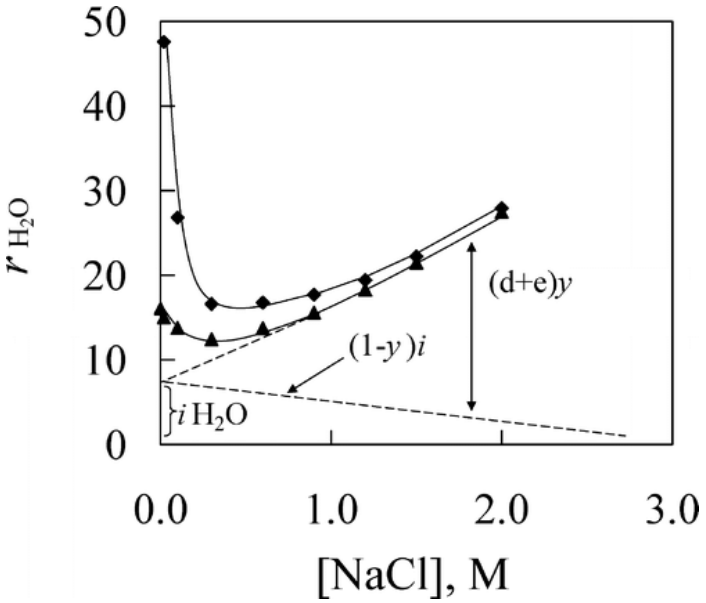

Figure 40. Fraction of water molecules in PDAC/PSS multilayers as a function of concentration. Reprinted (adapted) with permission from Schlenoff, J. B.; Rmaile, A. H.; Bucur, C. B. *Journal of the American Chemical Society* 2008, *130*, 13589-13597. Copyright 2008 American Chemical Society.

The contraction of the film observed in these studies and ejection of water from the film observed by Schlenoff *et al*. in Regime I is attributed to an increase in osmotic pressure. The behavior is otherwise termed the "polyelectrolyte effect" and has been previously detected in polyelectrolyte brushes.[86] Tran *et al.* demonstrated that in low ionic strength solutions or in pure water poly(styrenesulfonate, sodium salt) grafted polyelectrolyte brushes achieved an extended conformation due to the electrostatic repulsion and osmotic pressure.[87] The behavior of the film in Regime I can be paralleled to the "osmotic regime" which appears at low ionic strength and high grafting density. [87] Such behavior can also be explained in terms of changes in the Debye length. The Debye length can be described as the separation across which the electrostatic forces of the free

ions in solution affect the conformation of polyelectrolyte chains in solution .[88] It is also known to be inversely proportional to the square root of the ionic strength.[89] As such, divalent ions can be considered better screening agents due to the increased ionic strength as compared to monovalent ions at the same concentration. However, the magnitude of the changes observed appear too great to simply be a result of conformation changes of the polyelectrolyte chains and hydration effects are considered a more likely cause. In Regime II the expansion of the film described in these studies and the uptake of water presented in Schlenoff's work is referred to as the "anti polyelectrolyte effect" which is caused by extrinsic doping by the ions present in the surrounding solution and the incorporation of the associated waters into the film.[86]

One important difference to consider between the two studies is that the work presented by Schlenoff *et al.* was for a polyanion (PSS) terminated systems while the work demonstrated in this study is for polycation (PDAC) terminated films. We were not able to systematically investigate the PSS-terminated films because the resultant data was inconsistent. The films would behave either in an opposite fashion to the PDAC-terminated films or show no response at all to the changes in ion exposure.

The absence of a similar two-state effect in LbL films exposed to Na_2SO_4 could be due to Donnan principles. Donnan exclusion has been previously utilized in preparation of nanofiltration membranes using the LbL technique. These membranes are devised for the separation of monovalent and divalent ions. In order to form the membranes Harris *et al*. deposited PAH/PSS multilayers onto porous alumina substrates. [90] For a five bilayer film setting the polyanion (PSS) as the topmost layer was shown to

decrease the flux of SO_4^{2-} through the membrane from 2.2×10^{-8} to 9.9×10^{-9} mol-cm^{-2} s^{-1}. Figure 41 illustrates the drastic drop in the transport of multivalent salts, shown by the reduction in conductivity, through the membrane. [90]

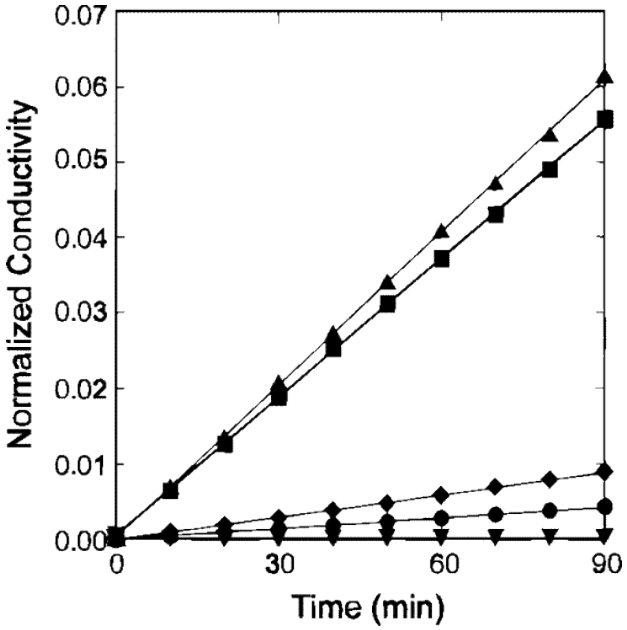

Figure 41. Normalized conductivity through a $(PAH/PSS)_5$ membrane as a function of time. Triangles = KCl; Squares = KNO_3; Diamonds = K_2SO_4; Circles = $K_2Ni(CN)_4$; Upside down Triangles = $K_3Fe(CN)_6$. Reprinted (adapted) with permission from Harris, J. J.; Stair, J. L.; Bruening, M. L. *Chemistry of Materials* 2000, *12*, 1941-1946. Copyright 2000 American Chemical Society.

The preferential rejection of the divalent ions from the film is caused by the electrostatic repulsion between the membrane bearing a negative charge of the topmost layer and ions of the same charge, or Donnan exclusion.[90] The experiments showed no significant effect of film thickness (or layer pair number) on the selectivity of the membranes once

the film fully coats the membranes; which suggests that, the selective penetration of ions occurs due to Donnan exclusion at the surface of the film.[90]

Even though a substantial portion of permeation studies focus on the PAH/PSS polyelectrolyte pair due to its high performance, some data is available for the PSS/PDAC system as comparison. In an investigation presented by Ouyang *et al*. nanofiltration membranes were prepared by assembling PDAC/PSS multilayers onto alumina substrates, similar to the previous study. $(PSS/PDAC)_4$-PSS and $(PSS/PDAC)_5$ films resulted in 38.2 and 42 % rejection rates of Mg^{2+} which also corresponded to 1.6 and 1.8 Na^{+}/Mg^{2+} selectivities, respectively.[91] Even though the performance of PSS/PAH membranes is significantly better with rejection rates for Mg^{2+} averaging in the 90 percentile,[91] the argument for the repulsion of a like charge by the topmost layer still stands.

This behavior led to the conclusion that the reverse effect of Donnan inclusion would allow the hydrated SO_4^{2-} ions to penetrate and fully saturate the LbL film. The lack of repulsion would also result in a lack of concentration dependence beyond some low threshold at which the film accepts the maximum amount of ions into its structure.

4.4.2: Mechanical Properties

In literature, viscoelastic properties of polyelectrolyte multilayers are often determined using atomic force microscopy (AFM). However, Salomäki *et al.* used QCM to determine the viscoelastic properties of PDAC/PSS films assembled using collection of counterions. The reported value of storage shear modulus for PDAC/PSS multilayers

assembled from NaCl is 8 ± 5 MPa which is in the same range of values reported in this work.[53] Additionally, this work demonstrates a reduction in shear modulus when the film is in contact with $CaCl_2$, $MgCl_2$ and Na_2SO_4 solutions, which have a higher number of associated water molecules as compared to NaCl. In other words as the water content within the films decreases the observed shear modulus increases. From previous studies water molecules have been shown to serve as plasticizers. Illustration in Figure 42 shows that the water molecules allow the polymer chains to move with more ease by increasing the amount of free volume. Stiffer PDAC/PSS complexes and multilayers have been observed after the discharge of water molecules under increasing osmotic stress.[92]

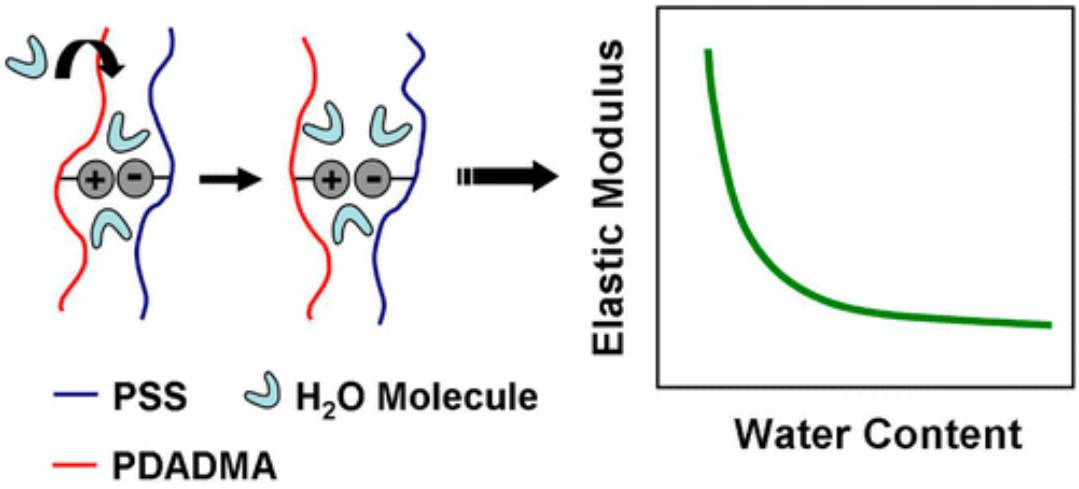

Figure 42. Schematic representation of the impact of water content on the elastic modulus and free volume within the multilayers. Reprinted from Hariri, H. H.; Lehaf, A. M.; Schlenoff, J. B. *Macromolecules* 2012, *45*, 9364-9372 an open access article.

5. RESULTS – THERMAL RESPONSE

5.1: Thermal Transition in Hydrated PDAC/PSS Assemblies

Previous measurements collected in our lab observed a thermal transition in hydrated poly(diallyldimethylammonium chloride) (PDAC) / poly(styrene sulfonate sodium salt) (PSS) multilayers when in the presence of NaCl. The thermal transition appears to be second order and resembles a glass transition temperature. Through molecular dynamic simulations it was determined that the thermal transition is not a classical glass transition but is associated with the PSS-water interactions. In order to further investigate the effect free ions have on the interactions between the sulfonate groups and water molecules LbL films were hydrated using $CaCl_2$, $MgCl_2$ and Na_2SO_4 and then analyzed using modulated differential scanning calorimetry (MDSC). The data presented in this chapter expands previous work by looking at the effect of ion type and ion concentration on the thermal transition.

Free-standing LbL films were prepared using an automated slide stainer (HMS series, Carl Zeiss, Inc.) on Teflon® substrates. The substrates were treated by sonication for 15 min in ethanol, then two rounds in 18.2 MΩ Milli-Q water prior to assembly. Film assembly proceeded by holding the substrates in PDAC solution for 15 min, followed by three rinses in Milli-Q water for 2, 1, and 1 min, respectively. The process was then repeated using PSS solution. PDAC and PSS solutions were dissolved in Milli-Q water

at a concentration of 1 mg/ml and ionic strength of 0.5 M NaCl was used for all solutions. After 140 layer pairs were assembled the samples were dried in ambient conditions overnight followed by additional drying under vacuum at 115 ^{o}C for 3 hours.

5.2: Concentration Dependence

MDSC (TA Instruments DSC Q200) was used to assess the presence of a thermal transition in hydrated LbL assemblies. Once the films were removed from the substrate they were hydrated with 36 wt% of $CaCl_2$, $MgCl_2$ or Na_2SO_4 solutions with concentrations ranging from 0.01 M to 2 M, and the total MDSC sample mass (film plus solution) ranged between 7 and 11 mg, depending on sample availability. The hydrated samples were sealed inside Tzero hermetic pans and lids (TA Instruments). Hydrated films were first allowed to equilibrate at 0 ^{o}C for 5 min then ramped from 0 ^{o}C to 115 ^{o}C at a rate of 2 ^{o}C/min with amplitude of 1.272 ^{o}C for a period of 60 s. The thermal cycle was repeated two times and the reported thermal transition (T_{tr}) values were taken as the inflection point in the second heating scan.

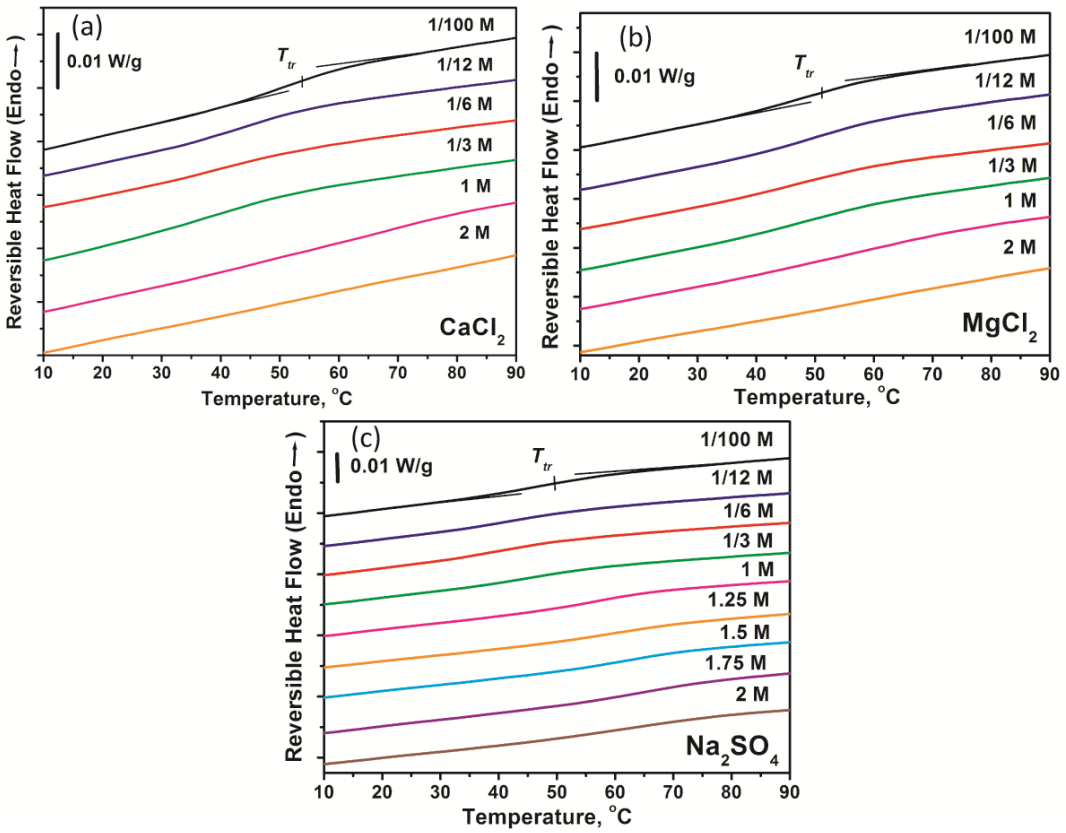

Figure 43. Effect of divalent ions on the thermal transition of $(PDAC/PSS)_{140}$ LbL films. MDSC measurements of free-standing LbL films hydrated to 36 wt% using solutions of (a) $CaCl_2$, (b) $MgCl_2$ and (c) Na_2SO_4 of varying concentrations. Data was shifted along the y-axis for clarity. Heating at 2 °C/min, amplitude of 1.272 °C for a period of 60 s. Second scan shown.

Figure 43 shows a thermal transition in PDAC/PSS multilayers hydrated using $CaCl_2$, $MgCl_2$ and Na_2SO_4 solutions. The transition is weak and resembles a glass transition in its shape. The thermal transition was observed in films hydrated with Na_2SO_4 solutions ranging in concentration from 0.01 M to 2 M, Figure 43c. However, when the films were hydrated using $CaCl_2$ and $MgCl_2$ the thermal transition could not be detected for concentrations above 1/3 M, Figure 43a-b.

Similar to the structural analysis, the thermal transition values were examined as a function of concentration in order to determine possible concentration dependence. As can be seen in Figure 44a the thermal transition values of LbL films hydrated using $CaCl_2$ solutions remained constant at about 44 – 51 ^oC within standard deviation for the full range of concentrations considered in this work. Films hydrated using $MgCl_2$ solutions also showed no concentration dependence. As shown in Figure 44c samples hydrated using Na_2SO_4 solutions up to a concentration of 1/6 M displayed a constant thermal transition at approximately 45 ^oC. However, at higher concentrations the thermal transition began to increase linearly with increasing concentration. This linear dependence can be written as $T_{tr} = 11.12\ C_{Na2SO4} + 44.01$ with an $R^2 = 0.94$.

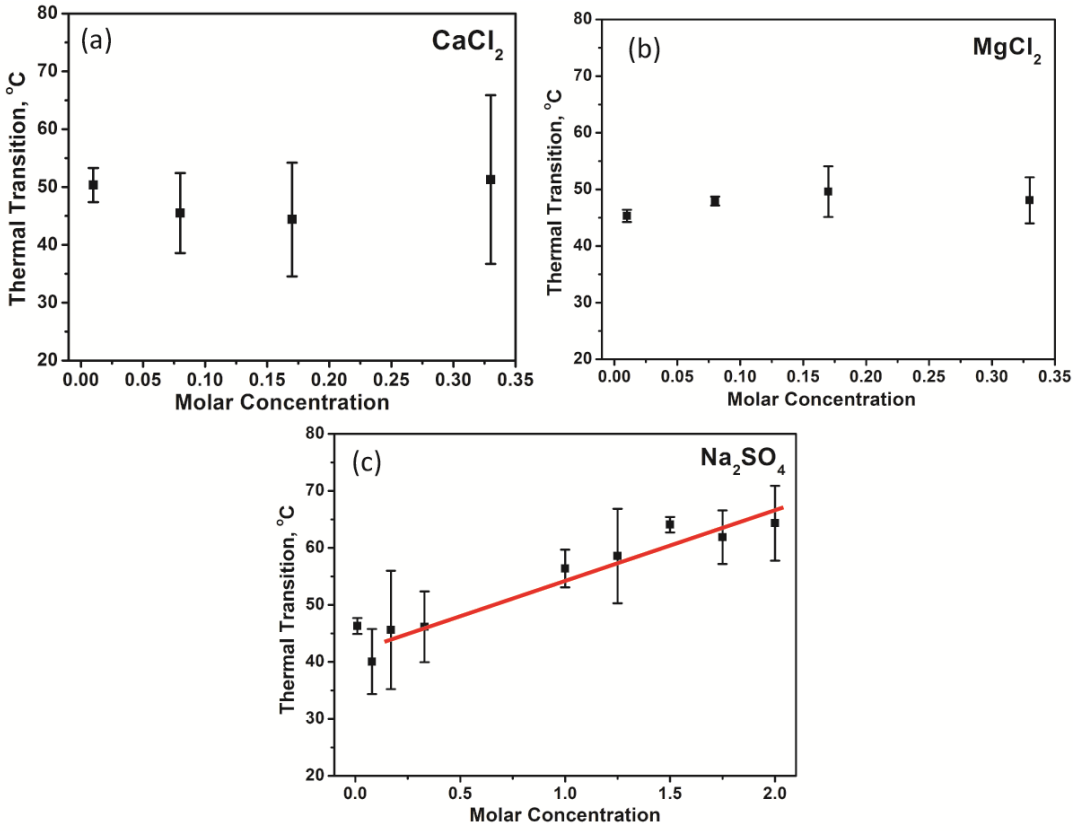

Figure 44. Concentration dependence of the thermal transition of hydrated LbL multilayer films in the presence of $CaCl_2$ (a) and Na_2SO_4 (b). The solid lines are drawn to help guide the eye and represent a linear fit of $T_{tr} = 11.12\ C_{Na2SO4} + 44.01$ ($R^2 = 0.94$). The error bars represent the standard deviation over at least three samples.

5.3: Discussion

The appearance of ionic strength dependence on the position of the thermal transition when hydrated with Na_2SO_4 solutions (but not $CaCl_2$ and $MgCl_2$) may be attributed to the kosmotropic nature of the SO_4^{2-} ion. Kosmotropes are referred to as "structure making" due to their ability to stabilize water structures and interactions. On the other hand, chaotropes are known as "structure breaking" because of their tendency

to disturb water structures.[93] SO_4^{2-}, Ca^{2+} and Mg^{2+} are more kosmotropic in reference to Cl^- and Na^+.[76] However, it has been previously claimed that anions have a stronger effect on water structures than cations.[94] As a kosmotrope SO_4^{2-} could have stronger interactions with the water molecules then the sulfonate group of PSS. As a result, with increasing concentration of Na_2SO_4 fewer PSS-H_2O bridges would form. Due the reduction of water interactions within the structure of the film acting as plasticizer more energy input would be necessary in order to observe increased chain mobility.

Another explanation could be based on strong doping effects by the divalent cations. Ca^{2+} and Mg^{2+} may be forming a large number of external compensation sites with the PSS chains in the bulk of the film which disrupts the PSS-H_2O bridges. In the low to intermediate concentration range (up to 1/3 M) enough water bridges still form for the thermal transition to be observed. At the ultra-high concentrations (1 M and above) the amount of external doping induces such a great disruption of the PSS-H_2O bridges that the transition can no longer be observed.

6. FUTURE WORK

6.1: FTIR Investigation of the Thermal Transition of LbL Assemblies in an Aqueous Environment

Future work will further investigate the effect of ions on the observed thermal transition in layer-by layer (LbL) assemblies by Fourier transform infrared spectroscopy (FTIR). To date there is no available spectroscopic evidence of the transition. This method allows investigation of the poly(styrene sulfonate sodium salt) (PSS)-H_2O interactions which holds features of the transition and would be affected by the presence of free ions. The emission band from the sulfonate groups can be monitored as a function of temperature. Shifts in wavenumber peak position due to faster vibration of molecules would provide further corroboration of the presence of the transition. The changes in absorbance could be used to discuss relative effect of monovalent versus divalent ions on molecular movement within the film. Figure 45 shows a schematic view of a set-up for the proposed experiments. An LbL film will be deposited onto an FTIR crystal using an external set-up following the same conditions as described previously. The film will then be immersed in solutions of different salts over a range of concentrations and allowed to equilibrate. FTIR spectra will then be collected with increasing temperature. A sample immersed in 0.5 M NaCl solution will serve as the control.

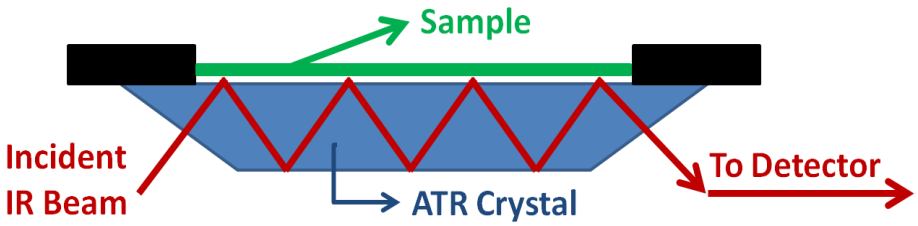

Figure 45. FTIR set-up

6.1.1: FTIR Background

FTIR is a characterization technique which operates by identifying the structural framework and electronic interactions of a presented sample. The technique has now been used to analyze specimens ranging from small molecules to tissues.[95] The infrared spectra are collected as footprints of the molecular vibrational energy of a provided sample. The infrared signal is then cataloged and matched to particular chemical structures based on the characteristic absorption bands.[95] One possible mode of vibrational energy is stretching; the oscillation frequency characteristic of two atoms undergoing this type of motion can be evaluated using the following equation

$$\upsilon = \frac{1}{2\pi c l}\sqrt{\frac{k(m_1 + m_2)}{m_1 m_2}}$$

where c_l is the speed of light, m_1 and m_2 are the atomic masses of the two atoms in motion and k is bond strength between the two atoms.[95]

FTIR has also been previously used to characterize LbL films. Jaber *et al.* used attenuated total internal reflectance FTIR (ATR-FTIR) in order to compare the level of water uptake and ion doping in poly(diallyldimethylammonium chloride) (PDAC) / PSS and poly(allylamine hydrochloride) (PAH) / PSS LbL films exposed to solutions of NaCl and $NaClO_4$.[96] As shown in Figure 46, PDAC/PSS films displayed a larger degree of ion incorporation compared to PAH/PSS multilayers as is indicated by the higher slope. The researchers concluded that lower $NaClO_4$ inclusion is a result of stronger interactions between the PAH and PSS chain segments.[96] The researchers also observed that the water content of the PAH/PSS films remained unaffected by the ionic strength both in the presence of NaCl and $NaClO_4$. On the other hand, PDAC/PSS presented a linear increase in water content with increasing $NaClO_4$ concentration and a two-mode behavior in the presence of NaCl.[96]

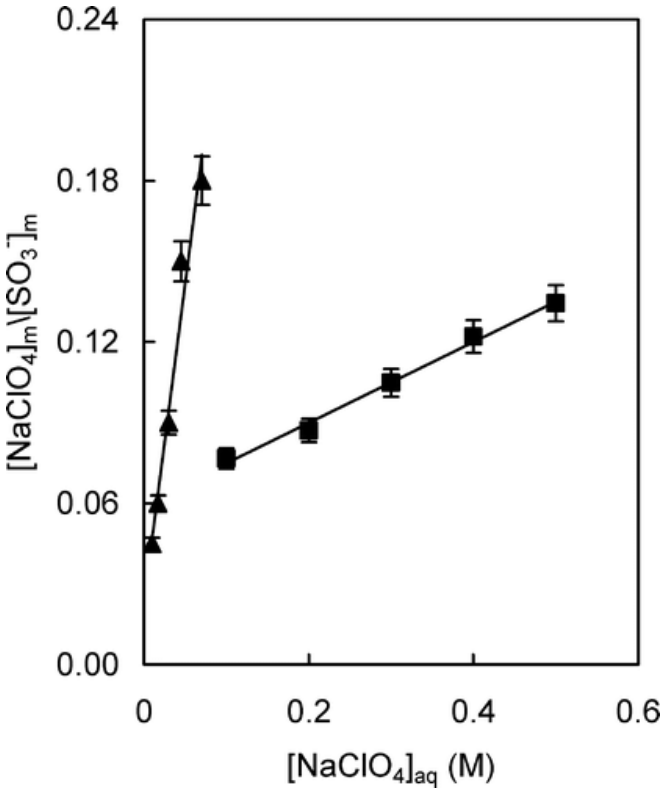

Figure 46. $NaClO_4$ incorporation into LbL film vs. solution concentration. Triangles = PDAC/PSS; Squares = PAH/PSS. Reprinted (adapted) with permission from Jaber, J. A.; Schlenoff, J. B. *Langmuir* 2007, *23*, 896-901. Copyright 2007 American Chemical Society.

In a separate study by Farhat *et al.* FTIR was used in order to track the ion exchange process within PDAC/PSS multilayers.[97] Figure 47 shows the steady increase in the amount of ions being incorporated into the film and providing extrinsic compensation as the concentration of the external solution increases. The fraction of ions involved in extrinsic compensation is designated by the variable *y*. [97] The solid curve represents a theoretical fit of the data assuming a fixed swelling constant. The dotted curve is obtained from the same theoretical expression but using a swelling constant that changes with the doping level according to a predefined function. [97] The researchers also point

out that even when the external solution is devoid of ions some extrinsic compensation is present within the film.[97]

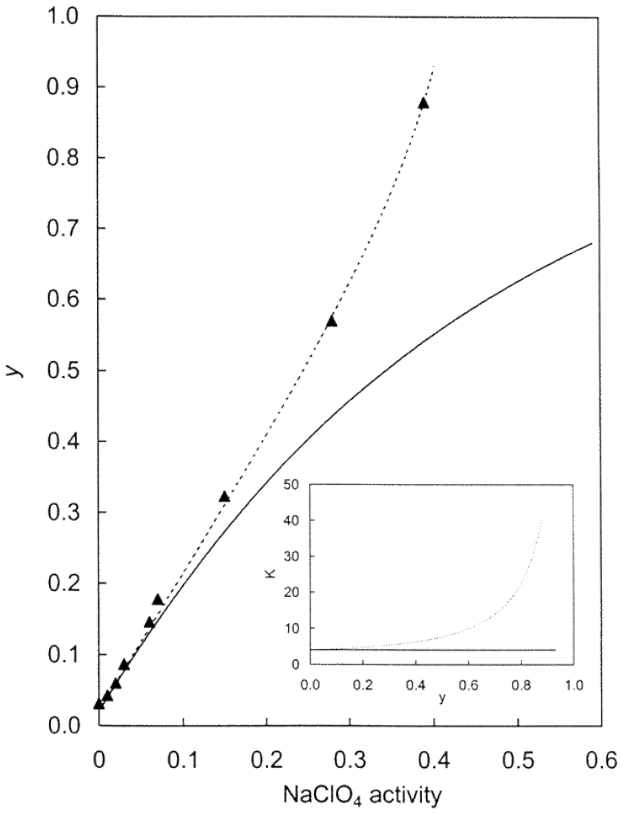

Figure 47. Doping level of a PDAC/PSS film with respect to $NaClO_4$ activity in solution. Reprinted (adapted) with permission from Farhat, T. R.; Schlenoff, J. B. *Journal of the American Chemical Society* 2003, *125*, 4627-4636. Copyright 2003 American Chemical Society.

6.2: Effect of Ion Exposure on the Structure of LbL Assemblies

Another avenue available for further exploration is to examine a wider collection of ions in solution and observe their effect on the post-assembly structure and thermal

behavior of LbL films. This study would be conducted in terms of the kosmotropic or chaotropic character of the selected ions.

Figure 48 shows the change in the entropy of water molecules, otherwise known as "mobility", as a function of the radius of the ions that the water is in contact with.[98] The mobility values were obtained from the apparent molecular weight measurements from a collection of aqueous solutions containing different ions. The solutions were passed through a column containing Sephadex G-10 and the molecular weight of the ions leaving the column was compared to the anhydrous molecular weight.[98] An increase in the molecular weight, negative entropy, indicates that water molecules are captured by the ion and travel with it along the column. However, if the apparent molecular weight is less than the anhydrous value, positive entropy, the interactions between the ion and the water molecules are weak and only exist temporarily.[98] Thus, the change in entropy shows a direct distinction between kosmotropic and chaotropic ions. Ions which bear a negative mobility value restrict the movement of water molecules, forcing the waters to order around the ion, are known as kosmotropes. Chaotropes have the opposite effect. These ions expand the movement of water molecules near them and carry a positive mobility value.[98]

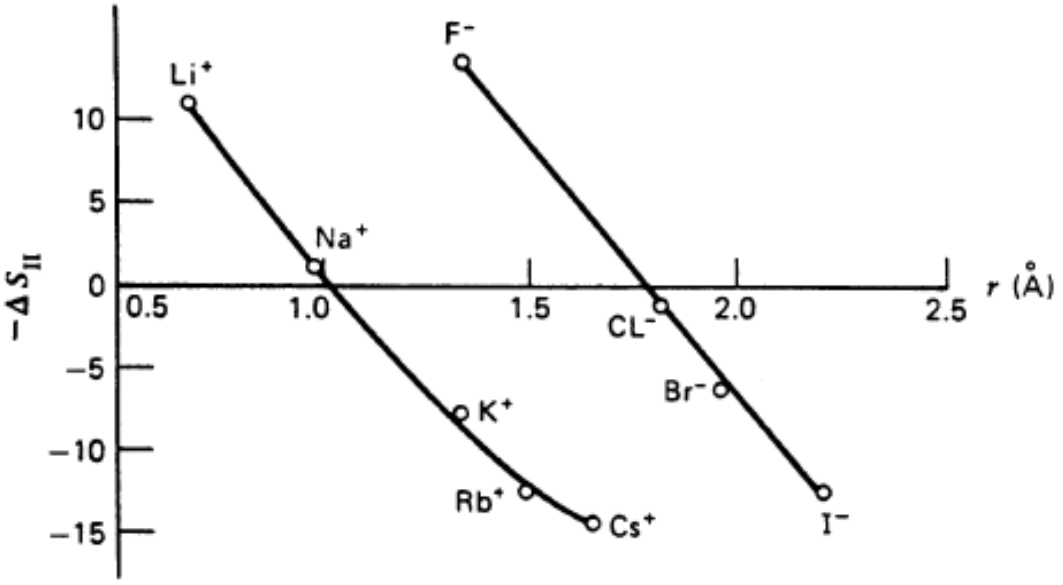

Figure 48. The change in entropy of water molecules as a result of addition of indicated ions as a function of the ion radius. Reprinted from *Biophysical Journal*, 72, Collins, K. D., Charge density-dependent strength of hydration and biological structure, 65-76, Copyright 1997, with permission from Elsevier.

Chaotropes and kosmotropes can also be distinguished by looking at the Jones-Dole viscosity B coefficient. The parameter represents waters' affinity to the ion. High B coefficient is characteristic of kosmotropes and low B coefficient is typical for chaotropes.[98]

The effect of ionic character has already been established for certain polyelectrolyte brushes. The Liu group looked at the effect of a group of anions on poly[2-(methacryloyloxy)ethyltrimethylammonium chloride] (PMETAC) brushes and a group of cations on poly(3-sulfopropyl methacrylate potassium) (PSPMA) brushes.[99] Figure 49 illustrates schematically the difference in the effect of kosmotropic and chaotropic ions on polyelectrolyte brushes. In the presence of chaotropic anions

PMETAC brushes collapsed due to charge compensation provided by the free ions in solution. Kosmotropic ions also led to a reduction in the extension of the brushes but to a lesser degree.[99] The kosmotropic ions interact strongly with the surrounding water molecules thus forcing them away from the polyelectrolyte brushes. The effect of the cations on PSPMA followed the same pattern but produced a weaker response.[99]

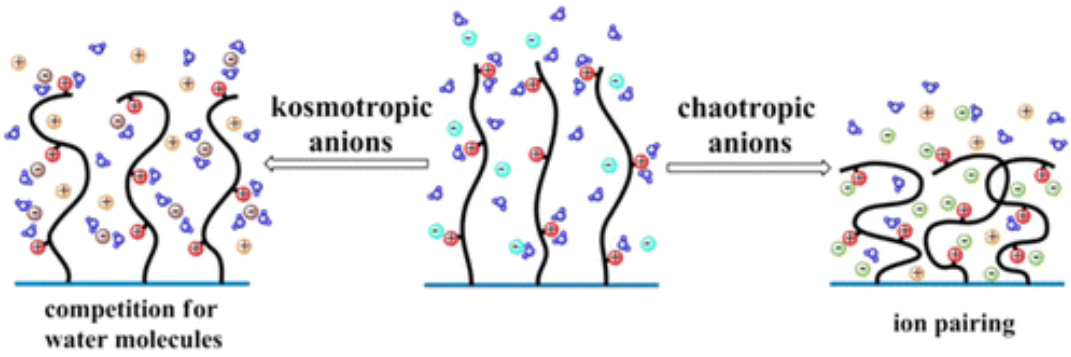

Figure 49. Schematic representation of polyelectrolyte brush collapse in the presence of free ions. Reprinted (adapted) with permission from Kou, R.; Zhang, J.; Wang, T.; Liu, G. *Langmuir* 2015, *31*, 10461-10468. Copyright 2015 American Chemical Society.

7. CONCLUSIONS

The effect of multivalent ions on the structure and thermal behavior of poly(diallyldimethylammonium chloride) (PDAC) / poly(styrene sulfonate sodium salt) (PSS) LbL assemblies was investigated. A contraction and stiffening of the films was observed using QCM-D when the solution in contact with the film was switched from $CaCl_2$ ($MgCl_2$ or Na_2SO_4) to NaCl. The structural change was reversible and repeatable as the film largely regained its original thickness and became softer upon ion exchange from NaCl to $CaCl_2$ ($MgCl_2$ or Na_2SO_4). The changes in thickness were found to be linearly dependent on concentration of $CaCl_2$ and $MgCl_2$. However, the concentration of Na_2SO_4 did not affect the expansion and contraction of the film despite resulting in overall larger magnitude difference. The detected structural changes were interpreted on the basis of Donnan exclusion principle and the differences in the hydration shells of the collection of ions in contact with the polyelectrolyte multilayers. Structural changes were also found to not be thickness dependent. Analysis of the viscoelastic properties led to the detection of a reduced shear modulus for films in contact with divalent ions as compared to monovalent ions. The reduction in shear points to a plasticization effect from water molecules penetrating into the film and assisting chain movement. A thermal transition was observed when free-standing PDAC/PSS assemblies were hydrated using $CaCl_2$, $MgCl_2$ and Na_2SO_4 solutions of varying concentrations. The position of the thermal transition shifted to higher temperatures with increasing Na_2SO_4 concentration;

while the concentration of $CaCl_2$ and $MgCl_2$ had no effect. These findings provide some fundamental insight into the effects of multivalent ions on PDAC/PSS multilayers which has hitherto been lacking in the field of LbL. In future work, we would like to apply the same experimental approach to systematically study a collection of ions bridging the kosmotropic and chaotropic regimes.

REFERENCES

1. Decher, G. *Science* **1997,** *277*, 1232-1237.
2. Hammond, P. T. *Current Opinion in Colloid & Interface Science* **1999,** *4*, 430-442.
3. Richardson, J. J.; Bjornmalm, M.; Caruso, F. *Science* **2015,** *348*, 411-+.
4. Schönhoff, M. *Current Opinion in Colloid & Interface Science* **2003,** *8*, 86-95.
5. Sukhishvili, S. A. *Current Opinion in Colloid & Interface Science* **2005,** *10*, 37-44.
6. Decher, G., Layer-by-Layer Assembly (Putting Molecules to Work). In *Multilayer Thin Films*, Wiley-VCH Verlag GmbH & Co. KGaA: 2012; pp 1-21.
7. Krasemann, L.; Tieke, B. *Materials Science and Engineering: C* **1999,** *8–9*, 513-518.
8. van Ackern, F.; Krasemann, L.; Tieke, B. *Thin Solid Films* **1998,** *327–329*, 762-766.
9. Laschewsky, A.; Mayer, B.; Wischerhoff, E.; Arys, X.; Bertrand, P.; Delcorte, A.; Jonas, A. *Thin Solid Films* **1996,** *284*, 334-337.
10. Decher, G.; Lehr, B.; Lowack, K.; Lvov, Y.; Schmitt, J. *Biosensors & Bioelectronics* **1994,** *9*, 677-684.
11. Yang, X.; Johnson, S.; Shi, J.; Holesinger, T.; Swanson, B. *Sensors and Actuators B-Chemical* **1997,** *45*, 87-92.
12. Langer, R. *Nature* **1998,** *392*, 5-10.

13. Peyratout, C. S.; Dahne, L. *Angewandte Chemie-International Edition* **2004,** *43*, 3762-3783.

14. Qiu, X.; Leporatti, S.; Donath, E.; Möhwald, H. *Langmuir* **2001,** *17*, 5375-5380.

15. Richardson, J. J.; Björnmalm, M.; Caruso, F. *Science* **2015,** *348*.

16. Johnston, A. P. R.; Cortez, C.; Angelatos, A. S.; Caruso, F. *Current Opinion in Colloid & Interface Science* **2006,** *11*, 203-209.

17. Sukhorukov, G. B.; Antipov, A. A.; Voigt, A.; Donath, E.; Möhwald, H. *Macromolecular Rapid Communications* **2001,** *22*, 44-46.

18. Georgieva, R.; Moya, S.; Hin, M.; Mitlöhner, R.; Donath, E.; Kiesewetter, H.; Möhwald, H.; Bäumler, H. *Biomacromolecules* **2002,** *3*, 517-524.

19. Mateos, A. J.; Cain, A. A.; Grunlan, J. C. *Industrial & Engineering Chemistry Research* **2014,** *53*, 6409-6416.

20. Sung, C.; Hearn, K.; Reid, D. K.; Vidyasagar, A.; Lutkenhaus, J. L. *Langmuir* **2013,** *29*, 8907-8913.

21. Seo, J.; Lutkenhaus, J. L.; Kim, J.; Hammond, P. T.; Char, K. *Langmuir* **2008,** *24*, 7995-8000.

22. Shiratori, S. S.; Rubner, M. F. *Macromolecules* **2000,** *33*, 4213-4219.

23. Yoo, D.; Shiratori, S. S.; Rubner, M. F. *Macromolecules* **1998,** *31*, 4309-4318.

24. Gopinadhan, M.; Ahrens, H.; Günther, J.-U.; Steitz, R.; Helm, C. A. *Macromolecules* **2005,** *38*, 5228-5235.

25. Salomäki, M.; Vinokurov, I. A.; Kankare, J. *Langmuir* **2005,** *21*, 11232-11240.

26. Tan, H. L.; McMurdo, M. J.; Pan, G.; Van Patten, P. G. *Langmuir* **2003,** *19*, 9311-9314.

27. Dubas, S. T.; Schlenoff, J. B. *Macromolecules* **1999,** *32*, 8153-8160.

28. Lvov, Y.; Antipov, A. A.; Mamedov, A.; Möhwald, H.; Sukhorukov, G. B. *Nano Letters* **2001,** *1*, 125-128.

29. Guzman, E.; Ritacco, H.; Rubio, J. E. F.; Rubio, R. G.; Ortega, F. *Soft Matter* **2009,** *5*, 2130-2142.

30. Liu, G.; Zou, S.; Fu, L.; Zhang, G. *The Journal of Physical Chemistry B* **2008,** *112*, 4167-4171.

31. Liu, G.; Hou, Y.; Xiao, X.; Zhang, G. *The Journal of Physical Chemistry B* **2010,** *114*, 9987-9993.

32. Dressick, W. J.; Wahl, K. J.; Bassim, N. D.; Stroud, R. M.; Petrovykh, D. Y. *Langmuir* **2012,** *28*, 15831-15843.

33. Salomäki, M.; Tervasmäki, P.; Areva, S.; Kankare, J. *Langmuir* **2004,** *20*, 3679-3683.

34. Mermut, O.; Barrett, C. J. *The Journal of Physical Chemistry B* **2003,** *107*, 2525-2530.

35. Itano, K.; Choi, J.; Rubner, M. F. *Macromolecules* **2005,** *38*, 3450-3460.

36. Hiller, J. A.; Rubner, M. F. *Macromolecules* **2003,** *36*, 4078-4083.

37. Tanchak, O. M.; Barrett, C. J. *Chemistry of Materials* **2004,** *16*, 2734-2739.

38. Ramos, J. J. I.; Llarena, I.; Moya, S. E. *Journal of Polymer Science Part A: Polymer Chemistry* **2011,** *49*, 2346-2352.

39. Köhler, K.; Biesheuvel, P. M.; Weinkamer, R.; Möhwald, H.; Sukhorukov, G. B. *Physical Review Letters* **2006,** *97*, 188301.

40. Dubas, S. T.; Schlenoff, J. B. *Langmuir* **2001,** *17*, 7725-7727.

41. Köhler, K.; Shchukin, D. G.; Möhwald, H.; Sukhorukov, G. B. *The Journal of Physical Chemistry B* **2005,** *109*, 18250-18259.

42. Kügler, R.; Schmitt, J.; Knoll, W. *Macromolecular Chemistry and Physics* **2002,** *203*, 413-419.

43. Parveen, N.; Schönhoff, M. *Macromolecules* **2013,** *46*, 7880-7888.

44. Schwarz, B.; Schönhoff, M. *Langmuir* **2002,** *18*, 2964-2966.

45. Wong, J. E.; Rehfeldt, F.; Hänni, P.; Tanaka, M.; Klitzing, R. v. *Macromolecules* **2004,** *37*, 7285-7289.

46. Zan, X.; Hoagland, D. A.; Wang, T.; Peng, B.; Su, Z. *Polymer* **2012,** *53*, 5109-5115.

47. Salomäki, M.; Kankare, J. *Macromolecules* **2008,** *41*, 4423-4428.

48. Zhang, Y.; Furyk, S.; Bergbreiter, D. E.; Cremer, P. S. *Journal of the American Chemical Society* **2005,** *127*, 14505-14510.

49. Dodoo, S.; Steitz, R.; Laschewsky, A.; von Klitzing, R. *Physical Chemistry Chemical Physics* **2011,** *13*, 10318-10325.

50. Heuvingh, J.; Zappa, M.; Fery, A. *Langmuir* **2005,** *21*, 3165-3171.

51. Mueller, R.; Köhler, K.; Weinkamer, R.; Sukhorukov, G.; Fery, A. *Macromolecules* **2005,** *38*, 9766-9771.

52. Jaber, J. A.; Schlenoff, J. B. *Chemistry of Materials* **2006,** *18*, 5768-5773.

53. Salomäki, M.; Laiho, T.; Kankare, J. *Macromolecules* **2004,** *37*, 9585-9590.

54. Huber, R. G.; Fuchs, J. E.; von Grafenstein, S.; Laner, M.; Wallnoefer, H. G.; Abdelkader, N.; Kroemer, R. T.; Liedl, K. R. *The Journal of Physical Chemistry B* **2013,** *117*, 6466-6472.

55. Vidyasagar, A.; Sung, C.; Gamble, R.; Lutkenhaus, J. L. *ACS Nano* **2012,** *6*, 6174-6184.

56. Yildirim, E.; Zhang, Y.; Lutkenhaus, J. L.; Sammalkorpi, M. *ACS Macro Letters* **2015,** *4*, 1017-1021.

57. Sung, C.; Hearn, K.; Lutkenhaus, J. *Soft Matter* **2014,** *10*, 6467-6476.

58. Puhr, J. T.; Swerdlow, B. E.; Reid, D. K.; Lutkenhaus, J. L. *Soft Matter* **2014,** *10*, 8107-8115.

59. Bianco, M.; Aloisi, A.; Arima, V.; Capello, M.; Ferri-Borgogno, S.; Novelli, F.; Leporatti, S.; Rinaldi, R. *Biosensors and Bioelectronics* **2013,** *42*, 646-652.

60. Dixon, M. C. *Journal of Biomolecular Techniques : JBT* **2008,** *19*, 151-158.

61. Konash, P. L.; Bastiaans, G. J. *Analytical Chemistry* **1980,** *52*, 1929-1931.

62. Höök, F.; Vörös, J.; Rodahl, M.; Kurrat, R.; Böni, P.; Ramsden, J. J.; Textor, M.; Spencer, N. D.; Tengvall, P.; Gold, J.; Kasemo, B. *Colloids and Surfaces B: Biointerfaces* **2002,** *24*, 155-170.

63. Deakin, M. R.; Buttry, D. A. *Analytical Chemistry* **1989,** *61*, 1147A-1154A.

64. Elam, J. W.; Groner, M. D.; George, S. M. *Review of Scientific Instruments* **2002,** *73*, 2981-2987.

65. Reviakine, I.; Johannsmann, D.; Richter, R. P. *Analytical Chemistry* **2011,** *83*, 8838-8848.

66. Sauerbrey, G. *Zeitschrift für Physik* **1959,** *155*, 206-222.

67. Eisele, N. B.; Andersson, F. I.; Frey, S.; Richter, R. P. *Biomacromolecules* **2012,** *13*, 2322-2332.

68. Ngai, K. L.; Plazek, D. J.; Rendell, R. W. *Rheologica Acta 36*, 307-319.

69. Thomas, L., Technical paper TP 006: Modulated DSC® paper# 1 why modulated DSC®. In *An overview and summary of advantages and disadvantages relative to traditional DSC*, TA Instruments: 2005; p 8.

70. Thomas, L. C.

71. Reid, D. K.; Alves Freire, M.; Yao, H.; Sue, H.-J.; Lutkenhaus, J. L. *ACS Macro Letters* **2015,** *4*, 151-154.

72. Berens, A. R.; Hodge, I. M. *Macromolecules* **1982,** *15*, 756-761.

73. Thomas, L. C. *New Castle (DE): TA Instruments* **2005**.

74. Thomas, L. C. *TA Instruments, New Castle, DE* **2005**.

75. Wei, J.; Hoagland, D. A.; Zhang, G.; Su, Z. *Macromolecules* **2016**.

76. Collins, K. D. *Biophysical journal* **1997,** *72*, 65.

77. Marcus, Y. *Journal of the Chemical Society, Faraday Transactions* **1991,** *87*, 2995-2999.

78. Marcus, Y. *Journal of the Chemical Society, Faraday Transactions* **1991,** *87*, 2995-2999.

79. Huang, X.; Schubert, A. B.; Chrisman, J. D.; Zacharia, N. S. *Langmuir* **2013,** *29*, 12959-12968.

80. Xiong, H.; Cheng, M.; Zhou, Z.; Zhang, X.; Shen, J. *Advanced Materials* **1998,** *10*, 529-532.

81. Zhang, G.; Ruan, Z.; Ji, S.; Liu, Z. *Langmuir* **2010,** *26*, 4782-4789.

82. Konradi, R.; Rühe, J. *Macromolecules* **2005,** *38*, 4345-4354.

83. Zavitsas, A. A. *The Journal of Physical Chemistry B* **2005,** *109*, 20636-20640.

84. Floris, F. M.; Persico, M.; Tani, A.; Tomasi, J. *Chemical Physics Letters* **1994,** *227*, 126-132.

85. Malinowski, E. R.; Knapp, P. S.; Feuer, B. *The Journal of Chemical Physics* **1966,** *45*, 4274-4279.

86. Schlenoff, J. B.; Rmaile, A. H.; Bucur, C. B. *Journal of the American Chemical Society* **2008,** *130*, 13589-13597.

87. Tran, Y.; Auroy, P.; Lee, L. T. *Macromolecules* **1999,** *32*, 8952-8964.

88. Carrara, S.; Iniewski, K., *Handbook of Bioelectronics: Directly Interfacing Electronics and Biological Systems*. Cambridge University Press: 2015.

89. Kirkwood, J. G.; Poirier, J. C. *The Journal of Physical Chemistry* **1954,** *58*, 591-596.

90. Harris, J. J.; Stair, J. L.; Bruening, M. L. *Chemistry of Materials* **2000,** *12*, 1941-1946.

91. Ouyang, L.; Malaisamy, R.; Bruening, M. L. *Journal of Membrane Science* **2008,** *310*, 76-84.

92. Hariri, H. H.; Lehaf, A. M.; Schlenoff, J. B. *Macromolecules* **2012,** *45*, 9364-9372.

93. Hribar, B.; Southall, N. T.; Vlachy, V.; Dill, K. A. *Journal of the American Chemical Society* **2002,** *124*, 12302-12311.

94. Evers, F.; Steitz, R.; Tolan, M.; Czeslik, C. *The Journal of Physical Chemistry B* **2009,** *113*, 8462-8465.

95. Berthomieu, C.; Hienerwadel, R. *Photosynthesis Research* **2009,** *101*, 157-170.

96. Jaber, J. A.; Schlenoff, J. B. *Langmuir* **2007,** *23*, 896-901.

97. Farhat, T. R.; Schlenoff, J. B. *Journal of the American Chemical Society* **2003,** *125*, 4627-4636.

98. Collins, K. D. *Biophysical Journal* **1997,** *72*, 65-76.

99. Kou, R.; Zhang, J.; Wang, T.; Liu, G. *Langmuir* **2015,** *31*, 10461-10468.